EFFECT OF COLUMN ASPECT RATIO ON PUNCHING STRENGTH OF CONCRETE FLAT-PLATES

by

Özlem Özden

B.S. in C.E., Boğaziçi University, 1998

Submitted to the Institute for Graduate Studies in Science and Engineering in partial fulfillment of the requirements for the degree of

Master of Science

in

Civil Engineering

Boğaziçi University

2001

ACKNOWLEDGMENTS

I owe special thanks to Professor Turan Özturan of Bogazici University, and Asst. Professor Şevket Özden of Kocaeli University, for their helpful guidance and endless encouragement throughout this thesis.

I am also grateful to Research Assistant Onur Ertaş for his support in preparing the specimens, data acquisition and testing phases of this study.

Funding provided by the Turkish Ready Mix Concrete Association and DOGA Engineering and Design Company is gratefully acknowledged.

I also would like to thank to Structures Laboratory technician Hasan Şenel, help-to-technician Hamdi Ayar, and Materials Laboratory Technician Ilyas Gültekin for their assistance during the experimental phase of this study. Without them, the experiments could not be completed.

Finally I would like to thank to my family for their continuous support and encouragement.

ABSTRACT

EFFECT OF COLUMN ASPECT RATIO ON PUNCHING STRENGTH OF CONCRETE FLAT-PLATES

The rapid increase in the number of flat-plate structures in the national building stock in the form of residential and office buildings, along with the requirements introduced by the new Turkish Earthquake Design Code, such as promoting the use of shear walls in high seismic regions, made it necessary to experimentally investigate the punching behavior and capacity of flat-plates with different column aspect ratios. The change in the dimensions and aspect ratios of the vertical load carrying members may have an influence on the capacity. Hence, the current design equations may be needed for further validation.

The experimental and analytical investigation performed in this study contains the behavior and capacity of flat-plates with different column aspect ratios. Besides, a T-shaped specimen was also tested for the same reason. The plate concrete was in the Normal Strength Concrete range, all the specimens were isolated internal panels and the load was applied concentrically, while the slab reinforcement ratio was kept constant among the specimens. Using the available test data in the literature and the data from the current investigation an attempt was made to modify the current design equations. Also, the post failure behavior and capacity of the specimens were studied and the available equations were validated.

ÖZET

KOLON BOYUT ORANLARININ BETONARME PLAKLARDA ZIMBALAMA DAYANIMINA ETKİSİ

Konut ve ofis tipi binalarda betonarme düz döşeme yapı sistemi hızla popular olmakta ve ülkemiz yapı stoğunda önemli bir yer edinmektedir. Yeni Türk Deprem Yönetmeliği'nin yüksek sismik riskin bulunduğu bölgelerde, düz döşemeli sistemlerde perde duvar kullanımını zorunlu hale getirmesi düz döşeme kolon birleşimlerinin değişik kolon boyut oranları ile yeniden incelenmesini ve halihazır tasarım denklemlerinin geçerliliğinin kontrolu gerekliğini gündeme getirmiştir.

Burada yapılan analitik ve deneysel çalışmada Normal Dayanımlı Beton'dan imal edilmiş düz döşemelerin zımbalama davranışlarının ve kapasitelerinin değişen kolon kesiti boyut oranları ile nasıl değiştiği incelenmiştir. Ayrıca, T-Kesitli kolonlar da bu çalışma kapsamında incelenmiştir. Konsantrik yüklemenin incelendiği deney elemanlarında, döşeme donatısı sabit tutulmuştur. Literatürdeki deney verileri ve bu çalışmanın sonuçları kullanılarak tasarım denklemlerinde modifikasyonlar önerilmiştir. Deney elemanlarının göçme sonrası yük kapasiteleri ve davranışları da bu çalışma kapsamında incelenmiştir.

TABLE OF CONTENTS

LIST OF FIGURES

LIST OF TABLES

LIST OF SYMBOLS

a	Shear span (shortest distance from the column edge to the supporting perimeter)
a_1	Half length of the punch perimeter on the longer side of the column according to TS-500
b	Column x-sectional dimension
d	Slab effective depth
D	Nominal bar diameter of plate flexural reinforcement
D_{sup}	Circular support diameter of the test specimens
E_{20}	Energy absorbed at 20 percent successive steps of the punching failure load
E_s	Modulus of Elasticity of rebar
E_t	Total energy absorbed until P_p, punching failure load level
f_c'	Concrete characteristic compressive strength, measured on 150x300 mm cylinders
f_{ctd}	Design tensile strength of concrete (TS-500)
f_{sp}	Split cylinder strength measured on 150x300 mm cylinders
f_y	Yield strength of plate flexural reinforcement
h	Column x-sectional dimension on the transverse direction
K_i	Initial flexural stiffness of the flat plate specimen
K_i^*	Initial flexural stiffness of the plate calculated by using the normalized (corrected) plate center deflection
K_{sc}	Secant flexural stiffness of the flat plate
K_{sc}^*	Secant flexural stiffness of the plate calculated by using the normalized (corrected) plate center deflection
K_t	Tangent flexural stiffness of the flat plate
K_t^*	Tangent flexural stiffness of the plate calculated by using the normalized (corrected) plate center deflection
m	Flexural capacity of a unit width of slab
P_{cr}	Flexural cracking load of the plate specimens

P_p	Experimental punching load
P_{re}	Residual load level of the test specimens
P_{re}^{c1}	Residual load capacity calculated with respect to Equation 6.14
P_{re}^{c2}	Residual load capacity calculated with respect to Equation 6.15
P_{TS}	Punching load capacity, calculated according to TS-500
r	Column dimension
r_{long}	Longer dimension of column stub x-section
r_{short}	Shorter dimension of column stub x-section
s^-	Spacing of slab compression reinforcement
s^+	Spacing of slab tension reinforcement
t	Slab thickness
u_p	Length of punching perimeter located at d/2 distance from the column stub
u_{pc}	Continuous punching perimeter located at d/2 distance away from the column stub; it is irrelevant to the column aspect ratio
u_{pTS}	Length of the punching perimeter calculated according to TS-500
v_c	Concrete shear strength at the time of punching
v_{c1}	Theoretical shear strength over the punching perimeter, u_{pTS}
v_{c2}	Theoretical shear strength over the punching perimeter, u_{pTS}
v_{c3}	Theoretical shear strength over the punching perimeter, u_{pc}
v_{cc}	Shear stress at the time of failure over a punching perimeter u_{pc}
v_{cts}	Experimental shear stress at the time of punching, over a punching perimeter calculated according to TS-500 (P_p/u_{pTS})
v_{TS}	Theoretical shear strength of concrete according to TS-500
w	Crack width on the plate
ΣA_s	Total steel x-sectional area passing through the punching perimeter
ΣA_{s1}	Total steel x-sectional area passing through the punching perimeter u_{pTS}
ΣA_{s2}	Total steel x-sectional area passing through the punching perimeter u_{pc}
α_s	Column location factor according to ACI-318
β_c	Column rectangularity factor according to ACI-318
δ_c	Plate center deflection

δ_c^*	Normalized (corrected) plate center deflection values with respect to a slab with D_{sup}=1500 mm
δ_{cr}	Plate center deflection at the flexural cracking load (P_{cr}) level
δ_{max}	Plate center deflection at which the test is tesrminated
δ_p	Plate center deflection at the experimental punching load (P_p) level
ε_y	Yield strain of plate flexural reinforcement
ϕ	Prefix indicating the rebar diameter in milimeters
ϕ_{slab}	Diameter of the slab flexural reinforcement
γ	Strength modification factor in case unbalanced moments exist

1. INTRODUCTION

The behavior of flat-plate systems, where the slabs are directly carried by the columns, are highly influenced by the behavior and the capacity of the plate-to-column connections. Three dimensional and complicated stress distribution over a pseoudo punching perimeter around the columns is a function of concrete strength, amount of flexural reinforcement, load eccentricity due to seismic excitations and uneven span loadings, and the dimensional ratios between both the column and plate, and the column aspect ratio.

The state of stress in punching failure may be defined as the excessive principal tensile stresses on the predefined punching perimeter. By its nature, the tensile failure of concrete is sudden and destructive, resulting a brittle type of failure. Several flat-plate buildings are failed during and after the construction under gravity loads. Some of the reported failures may be listed as below.

- Aselsan Building, Ankara, Turkey (1981) [1] : The low concrete strength and the removal of the lower storey shoring were listed as the main reason for the failure.
- Bayrampaşa Wholesale Food Market Hall, Istanbul, Turkey (1986) [2] : The concrete strength was only 50 percent of the design specified strength, at the time of the removal of the shoring.
- 16 Storey Building in Boston, USA (1971) [3] : Structural failure was due to the inadequate thickness of the flat-plate, along with the poor detailing.
- J.C.Penney Building, Alaska, USA (1964) [4] : The partial collapse of the building during the Alaska earthquake is related to the low energy dissipation capacity of the system although shear walls are used to resist the lateral forces.

A literature review on the topic reveals that, the design equations in the national building codes, do not thoroughly cover the variables affecting the connection behavior. Besides, the punching capacity of rectangular columns may need to be investigated in detail since the new generation national earthquake codes recommend the use of shear-walls in seismic regions.

2. LITERATURE REVIEW

2.1. General

The structural system, where slabs are carried directly by the columns, is called flat-slab systems, and the system may be constructed either with column capitals or with drop-panels. The special construction practice, where neither column capitals nor drop panels are used, is called in engineering jargon as flat-plate structures [5]. Flat-plate structural system is mostly favored due to the ease of workmanship, as a result economy in construction, and due to the architectural advantages, such as high modularity in floor space partitioning during the service life of the structure and the architectural convenience of the smooth ceiling. Flat-plate systems are also favored due to their fire protection and ease of piping [6].

Flat-plate type of construction has been in use since the beginning of this century [7, 8] and is mostly favored for medium rise residential and office type of buildings with relatively regular and small column spacing and with relatively light service loads. The major concern with the performance of the flat-plate structural system is the relatively higher inter-story drifts under seismic loads and its susceptibility to punching, which is defined as a local shear failure of the plate-to-column connection. At the connection region, the punching failure takes place when a plug of concrete over the lower column stub is pushed out of the concrete slab. The punching failure is mainly due to the excess of principal tensile stresses occurred in the concrete plate beyond the tensile strength of concrete itself [9].

The punching failure in the connection occurs due to the gravity loads with or without unbalanced moments caused either by uneven span loading or seismic type of lateral loads. The phenomenon of punching is being studied on sub-assemblies tested in the laboratories, and studied on the actual flat-plate buildings in the last century. The first field test on flat plate construction was performed in Deere and Webber Building at Minneapolis in 1910. During the test, it was reported that the strain measurements on the reinforcement and on the concrete were taken at various locations of the building [10].

Several buildings with various layouts were tested after the Deere and Webber building. Powers Building in Minneapolis (1911), Franks Building in Chicago (1911), Northwestern Glass Company Building in Minneapolis (1913), and others were all tested in order to verify the prevailing flat-plate punching design equations [11].

The first laboratory test on punching strength of column foundations was done by Talbot in 1913 and the phenomenon of punching was first introduced. In the following years experimental and analytical studies revealed the design parameters of the plate-to-column connections to a certain extend. In most of the experimental work, the isolated plate-to column sub-assemblies were tested for the capacity predictions [9, 12 - 15]. Besides, large-scale multi-panel specimens were also studied for the purpose of moment distribution and equivalent frame analysis [11, 16, 17]. Also, effect of moment reversals was studied in order to verify the effect of reversed cyclic earthquake type of loading on the connection capacity and behavior [18 - 20].

The available literature on the punching strength and behavior of the flat-plates reveals that the capacity and the behavior of the sub-assemblies are influenced by a wide range of variables, such as the concrete strength, reinforcement ratio, load eccentricity, dimensional ratios between the column stub and the plate, and the load reversals under certain level of slab service loads.

2.2. Factors Influencing the Punching Capacity

2.2.1. Concrete Compressive Strength

The procedures and the prime variables for punching strength capacity calculations in the national building design codes, are mostly applicable to the column-to-slab connections having Normal Strength Concrete (NSC), not exceeding 41 MPa [21]. The available research influencing the code equations [12] are mostly on plates with concrete compressive strength in the NSC range. It is claimed that, the ratio between the observed and the calculated load capacities are less conservative for higher concrete strengths [15, 22]. On the other hand, Bogazici tests [9] revealed that the design code equations [23, 24]

do not become less conservative with the increasing concrete strength. However, new design approaches and equations may be necessary for the punching strength predictions for the High Strength Concrete (HSC) ranging between 40 to 80 MPa [9].

The more complicated design equations, such as Moe's [12] is claimed to be overestimating the punching shear capacity of the HSC flat-plates [22]. These conclusions may be because of the prediction of the concrete shear strength by using the square root of the concrete compressive strength. The published research revealed that, using the cubic root of the concrete compressive strength generally yields better results [22, 25 - 28].

The improvement of concrete compressive strength may cause an increase in the punching shear resistance of the flat-plates, but may not necessarily imply a change of failure position [28]. Regardless of the concrete compressive strength, the failure surface may be defined over a perimeter at a distance of d/2 away from the column stubs [9]. The increase in concrete strength, positively influence the slab initial stiffness and delays the appearance of the initial radial cracks [9, 27]. However, the use of HSC in flat-plates results in a more brittle failure than NSC [9, 22, 27]. Although, there is a lack of data for the influence of slab holes in case of HSC plates, it is reported that the influence may be higher compared to the plates with NSC [28].

The ultimate shear stress in case of plate punching is nearly twice the value commonly used for beams. This increased strength is explained as the increased effectiveness of the dowel forces and the presence of compressive membrane forces and arch action caused by the non-failing portion of the plate [29]. Research in this field yields that, the arch action is more effective in plates of HSC [30].

2.2.2. Plate Flexural Reinforcement

There is not a general agreement among the researchers, on the effect of flexural reinforcement. A group of researchers claimed that, the punching shear strength of flat-plates was influenced by the amount, efficiency and the strength of the flexural reinforcement [31, 32]. METU tests revealed that, the number of bars and their spacing

within the punching zone were probably better parameters to consider the contribution of the flexural steel to punching strength [14]. Reported test results showed that the strength increases with decreasing bar spacing, keeping the slab flexural capacity constant. Bogazici Tests also concluded that, the amount of flexural reinforcement had a bearing on the punching strength of flat-plates, but this effect was relatively small compared to the effect of the concrete strength [9, 18].

The tension steel was reported to yield at or near the failure crack around the column stub [33]. Strain measurements on the tension reinforcement concluded that the flexural steel yielded at approximately 65 percent of the punching failure load, and the compression steel strain increased suddenly with the yielding of the tension steel [34, 35]. This may explain the increasing punching load with increasing slab reinforcement ratio at Bogazici tests [9, 18]. On the other hand, either too closely spaced re-bars or bars with bigger diameters inversely affected the punching load, and this may be due to a less uniform distribution of stresses around the punching perimeter and due to the anchorage problems [31, 36]. These experimental investigations may lead to a point where the design code equations should better use the amount of flexural reinforcement for the capacity calculations, regardless of the plate concrete strength [22, 27, 37].

On the other hand, the second group of researchers claimed that the effect of flexural reinforcement should better be ignored in the capacity calculations [26, 38, 39]. The increase in plate reinforcement or the concentration of reinforcement over the punching perimeter was claimed to be ineffective for the enhancement of the punching load.

The plate crack spacing and crack widths are reported to be influenced by the increase of the flexural reinforcement. Slabs with higher reinforcement contents generally exhibited closely spaced smaller cracks [9, 40]. Increased flexural reinforcement also increased the stiffness of the flat-plates, as a result decreasing the deflections [9, 12, 41, 42]. Although the test results reveal the positive effect of flexural reinforcement in punching capacity, the building codes generally neglects this effect in their design procedures and equations.

The phenomenon of residual load capacity after punching failure, which was experimentally investigated in Bogazici tests [9, 18] is highly influenced by the flexural steel content within the punching perimeter. Besides, the amount and detailing of the compression reinforcement has an influence on the post-failure behavior of the plate-to-column connections. In order to limit the progressive failures under service loads or seismic excitations, several researchers recommend to use slab compression reinforcement [4, 19, 43 - 45]

2.2.3. Load Eccentricity

Punching failures in the plate-to-column connections of the flat-plate structures are mainly occurred due to the excessive gravity loads with or without unbalanced moments caused by uneven span loading or lateral loads originating from wind or seismic actions [46]. The distribution of shear stresses over the punching perimeter is assumed to be uniform, in case of gravity loads. The distribution of shear stresses caused by the unbalanced moments is claimed to be non-uniform over the depth of the plate and throughout the punching perimeter [47].

The shear stresses caused by unbalanced moments are transferred via torsional stresses through the column sides parallel to the load eccentricity, and via bending forces through the column sides perpendicular to the load eccentricity. The percentage of unbalanced moment transferred through the bending resistance of the plate may well be assumed to be 60 percent out of the total unbalanced moment [13]. This idealization of shear transfer is used in some of the building design codes such as TS-500 [24], while the percentage value is chosen as a variable dependent on the column aspect ratio in ACI-318 [23]. It is reported that the changing percentage approach of ACI-318 is significantly underestimating the actual distributions [48, 49].

Experimental studies on isolated plate-to-column sub assemblies, was reported to be representative for the behavior of the connections within the overall structure [50]. The tests on interior column stubs under monotonically increasing eccentric punching loads, as well as reversed cyclic loads, revealed that the punching capacity of the connection

decreased with increasing load eccentricities [9, 18]. Besides, the behavior of the connection under seismic excitations was reported to be influenced by the flexural capacity of the connection itself [20].

2.2.4. Dimensional Ratios and Column Rectangularity

Experimental and analytical research on the effect of column rectangularity and dimensional ratios of the column-to-plate connections revealed that the shear strength is closely related to the above-mentioned variables. The concrete shear capacity at the connection both depends on the ratio between the column dimension and the slab depth (r/d), and the aspect ratio (b/h) of the column itself.

As the column dimension gets bigger with respect to the slab depth, in other words, as the punching perimeter increases while the plate depth is constant, the shear strength of connection decreases [12, 26, 37, 51, 52]. For typical small values of r/d, the shearing surface is well confined with the non-yielding portion of the flat-plate around the connection via in-plane membrane stresses. The confinement of the punching region is likely to be reduced for higher r/d ratios [43]. This may also be observed in the tests specimens where the plates are restrained against lateral expansion, as a result the in-plane membrane forces are induced via the test set-up [53].

The effect of column rectangularity on the connection stresses arises as the stress concentrations increase on the corners and the shorted edges of the rectangular columns. The research on the topic revealed that concrete shearing stresses and bending moments increases as the column rectangularity gets above 2.5; for square like columns stresses are more uniformly distributed [12, 54, 55]. The bending moments, and thus the steel stresses, on the shorter edge of the column stub increases rapidly while the column aspect ratio increases.

2.3. Design Code Approaches for Punching Capacity

2.3.1. Turkish Building Code (TS-500) Approach

Turkish Building Code, TS-500 [24], assumes a punching perimeter located at d/2 distance from the column stub, in punching capacity calculations (Figure 2.1). The surface, which is related to the depth of the plate, is assumed to be able to transfer the shear stresses induced by the shearing forces and the unbalanced moments. The length of the punching perimeter is related to the aspect ratio of the column stub and the depth of the flat-plate (Figure 2.1-a,b) in rectangular columns, while the perimeter is assumed to be passing through a boundary, which is located at a minimum distance of d/2 from the edges or corners of a non-rectangular column stub (Figure 2.1-c).

The variable distance, a_1 for the rectangular column stubs is calculated according to Equation 2.1, as a result the punching capacity is calculated by using Equation 2.2. The shear strength term f_{ctd} is bigger then the shear strength of the beams, since it is assumed that the non-yielding portion of the flat-plates are confining the concrete in the punching cone, hence the strength is higher in this region (Equation 2.3).

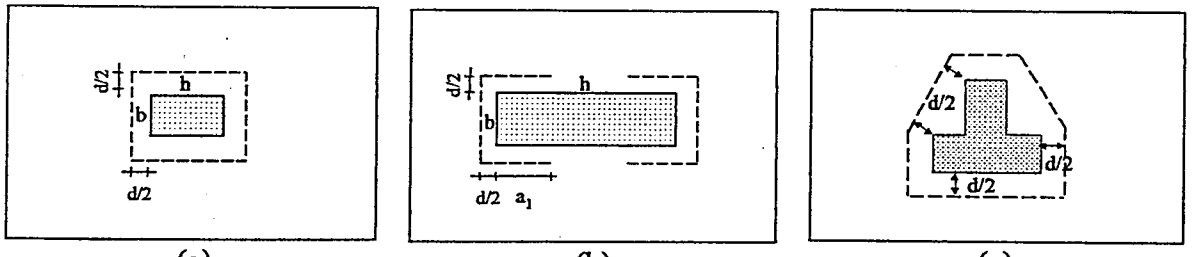

Figure 2.1. Punching perimeter definition for TS-500

Load eccentricity, in other words the effect of unbalanced moment, is considered via the variable γ as indicated in Equation 2.2, where it takes the value of unity for concentric punching.

$$a_1 \le \begin{pmatrix} h/2 \\ 2*b \end{pmatrix} \tag{2.1}$$

$$P_{TS} = \gamma * f_{ctd} * u_p * d \tag{2.2}$$

$$f_{ctd} = \frac{0.35}{1.5} * \sqrt[2]{f_c'} \tag{2.3}$$

2.3.2. American Concrete Institute (ACI 318) Approach

Punching load capacity calculations in ACI-318 [23] also considers the column rectangularity. Different than that of the TS-500 approach, ACI-318 modifies the concrete punching strength, v_c with respect to the column rectangularity value,β (Equation 2.4). Also, the shear strength of the connection is assumed to be related to the location of the column stub (Equation 2.5).

$$v_c = \text{smallest of} \begin{cases} (1+\frac{2}{\beta_c})\frac{\sqrt[2]{f_c'}}{6} \\ (2+\frac{\alpha_s d}{u_p})\frac{\sqrt[2]{f_c'}}{12} \\ \frac{1}{3}\sqrt[2]{f_c'} \end{cases} \tag{2.4}$$

$$\beta_c = \frac{\text{column longside}}{\text{column shortside}} \qquad \alpha_s = \begin{cases} 40 : \text{interior columns} \\ 30 : \text{edge columns} \\ 20 : \text{corner columns} \end{cases} \tag{2.5}$$

The punching perimeter, similar to TS-500, is located at d/2 distance from the column stub, and it is assumed to be continuous regardless of the column aspect ratio, since the v_c inherently has this effect.

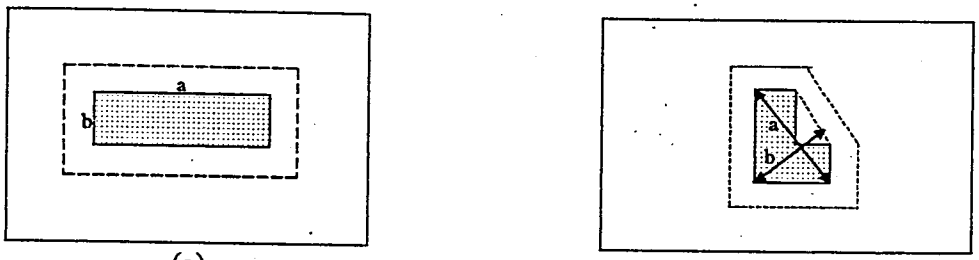

(a) (b)

Figure 2.2 – Punching perimeter definition for ACI-318

3. OBJECT AND SCOPE OF STUDY

When the design equations and detailing regulations in the national building codes are investigated, it is observed that they are mostly empirical and calibrated with respect to some certain test results available in the literature. Moreover, the number of tests, having the effect of column aspect ratio as a variable on the punching strength, is scarce. Most of the experimental investigation is devoted to the square columns. Besides, the available tests are all on rectangular and circular column stubs, excluding the behavior of T or L shaped column-to-plate connections.

In this study, the column aspect ratio is chosen as the main variable of the experimental investigation. The available test data in the literature is also elaborated and investigated along with the test results of the current investigation. The main purpose may be highlighted as the validation of the current building design code equations and procedures for rectangular and T-shaped column-to-plate connection capacities.

During the tests, the cracking pattern, which is the sign of the imminent failure, and residual load capacities are also investigated together with the punching capacities of the specimens.

The effect of concrete strength, plate flexural reinforcement, load eccentricity, existence and dimension of the plate holes are out of the scope of the current experimental and analytical investigation. An attempt was made to predict the punching capacities of the specimens via a set of newly proposed equations. Moreover, the residual load capacity calculation procedures and equations derived for the square columns are validated for the rectangular column stubs with higher column aspect ratios.

4. EXPERIMENTAL PROGRAM

4.1. Materials

4.1.1. Concrete

For the test specimens, Normal Strength Concrete (NSC) with a nominal compressive cylinder strength (f_c') of 25 MPa, was used. The maximum aggregate size of the concrete mix was 20 mm. The concrete used was obtained from a local ready-mix concrete company, and delivered wet, to the Structures Laboratory of Bogazici University. The concrete mix design supplied by the ready-mix concrete company is given in Table 4.1.

Table 4.1. Mixture proportioning of the ready-mix concrete used

Material	Amount (kg/m3)
Water	191
Cement	254
Sand 1	505
Sand 2	340
Crushed Stone No:1	430
Crushed Stone No:2	610

4.1.2. Reinforcing Bars

Two different sizes of deformed steel bars were used for the reinforcement of the four flat-plate specimens. The ϕ10 deformed re-bars, with a nominal bar diameter (D) of 10 mm, were used for the slab flexural reinforcement, while ϕ14 deformed re-bars were used as the column longitudinal reinforcement for the column stubs of the specimens. The column stubs were confined with ϕ10 steel bars. Three samples from each re-bar group were tested and the tensile test results were averaged before they were used in the design

calculations of the specimens. Riehle Universal Testing Machine, equipped with a load cell and two, Linear Variable Differential Transducers (LVDT), was used to conduct the rebar tension tests. The experimental mechanical properties of the re-bars are given in Table 4.2 and the stress-strain curves of the both sizes of the re-bars are shown in Figure 4.1 and Figure 4.2.

Table 4.2. Mechanical properties of deformed re-bars

Re-Bars Designation	ϕ10	ϕ14
Nominal Diameter (mm)	10	14
Nominal X-Area (mm^2)	78,5	153,9
f_y (MPa)	547	471
ε_y (mm/mm)	0,0026	0,0025
E_s (MPa)	210,400	181,500

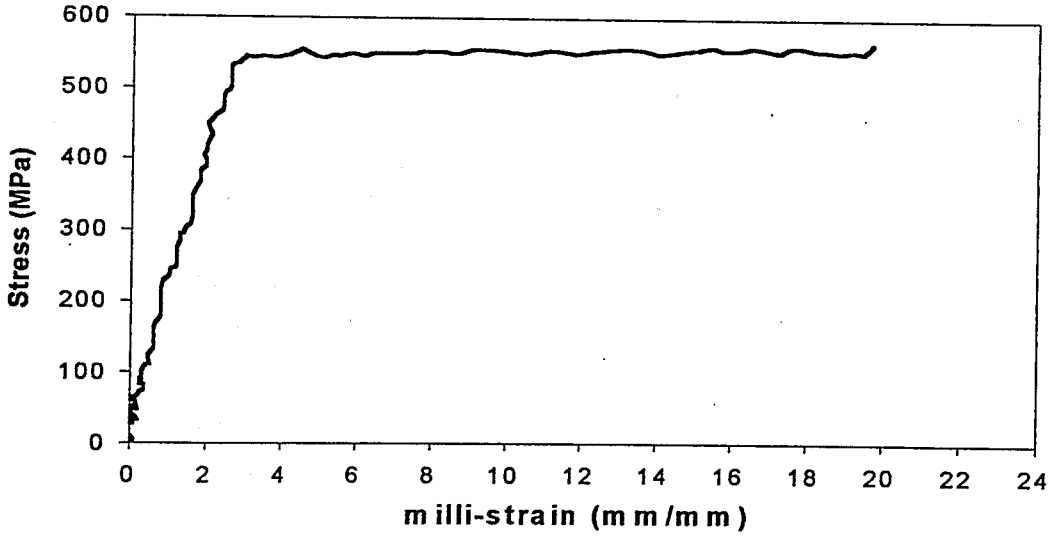

Figure 4.1. Stress-strain curve for ϕ10 re-bars

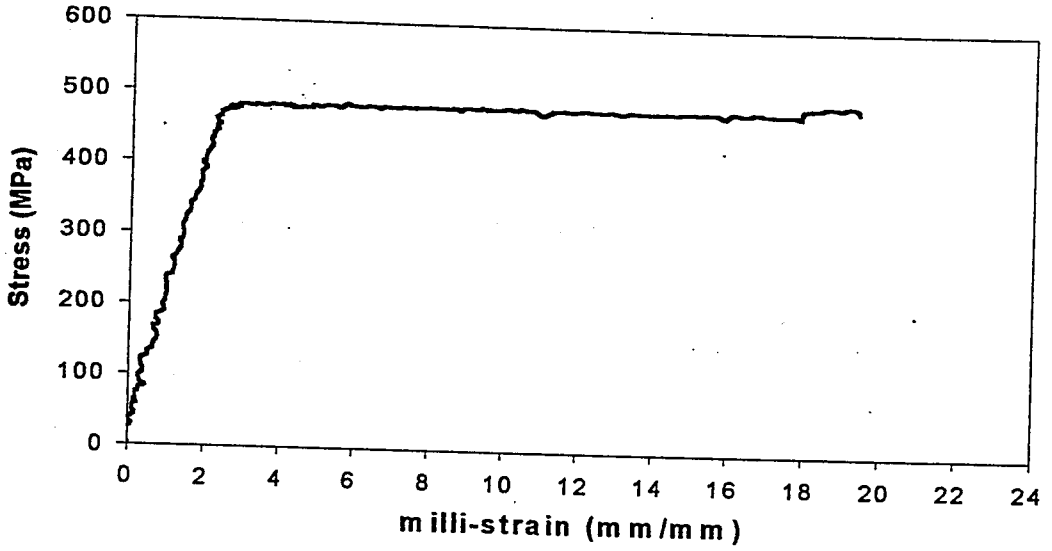

Figure 4.2. Stress-strain curve for ϕ14 re-bars

4.2 Test Specimens

Within the content of this thesis, four reinforced concrete circular flat-plate specimens were cast and tested in order to investigate the effect of column rectangularity on the punching behavior and strength of NSC flat-plates. Every specimen had a reinforced concrete column stub on the compression side of the plate (top), with different aspect ratios. The specimens were named according to their column shapes, and specimen name-tag list is given in Table 4.3.

The slab thickness of the specimens were kept constant at t=120 mm. On the other hand, every specimen had different column dimensions and support diameters. All specimens had constant shear span to depth ratio, resulting in different slab support diameters (D_{sup}) with changing column dimensions. Before the production of the test specimens, the calculated punching capacity values which were obtained through the TS-500 [24] design equations (P_{TS}) were calculated by using the nominal concrete compressive strength in order to check the available loading capacity of the test set-up. For the current investigation, the calculated punching perimeter, u_p according to the TS-500 design method was set to 1600 mm, and the ratio of the shortest distance from the column stub to support perimeter to the effective depth of the slab, in other words shear

span to depth ratio, was set to five in all test specimens. Specimen design data are given in Table 4.4.

Table 4.3. Specimen name-tag list

Specimen Definition	Specimen Name-Tag
Specimen with square column	OOSQ
Specimen with rectangular column	OORC
Specimen with shear wall	OOSW
Specimen with T-shape column	OOTE

Table 4.4. Specimen design values and nominal capacities

Specimen	**OOSQ**	**OORC**	**OOSW**	**OOTE**
t (mm)	120	120	120	120
d (mm)	100	100	100	100
D_{sup} (mm)	1300	1480	1720	1464
r_{short} (mm)	300	120	120	120
r_{long} (mm)	300	480	720	463
f_c' (MPa)	25	25	25	25
ϕ_{slab} (mm)	10	10	10	10
f_y (MPa)	547	547	547	547
s^+ (mm)	75	75	75	75
s^- (mm)	150	150	150	150
u_p (mm)	1600	1600	1600	1600
P_{TS} (kN)	313.05	313.05	313.05	313.05

ϕ10 deformed re-bars were used as slab tension and compression reinforcement yielding a constant reinforcement ratio for every specimen. The slab tension and compression reinforcement ratios were 1.05 and 0.52 percent, respectively. Column stubs were confined also with ϕ10 steel bars at every 6 cm. Column stub dimensions and reinforcement layout of the specimens are given in Table 4.5.

Table 4.5. Column dimensions and column reinforcement layout

Specimen Designation	Column Dimension and Reinforcement
OOSQ	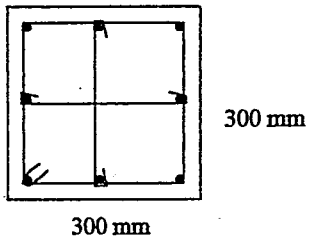
OORC	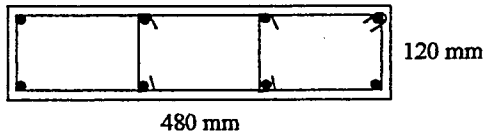
OOSW	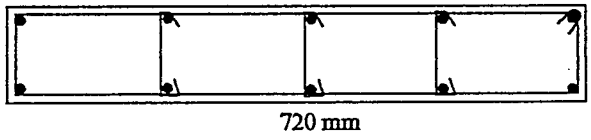
OOTE	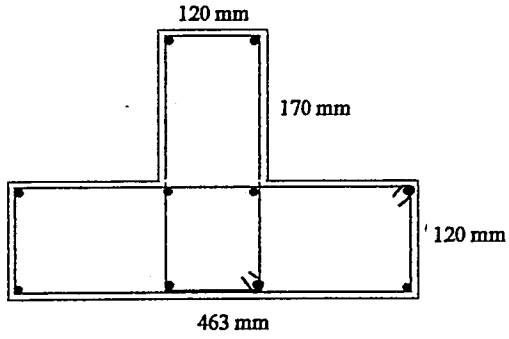

Flat-plate specimens had two layers of reinforcement mesh (Figure 4.3). The top reinforcement according to the testing set-up was the compression reinforcement and it was designed to be half of the tension reinforcement. As stated before, the tension reinforcement ratio of all the four specimens was kept constant at 1.05 percent.

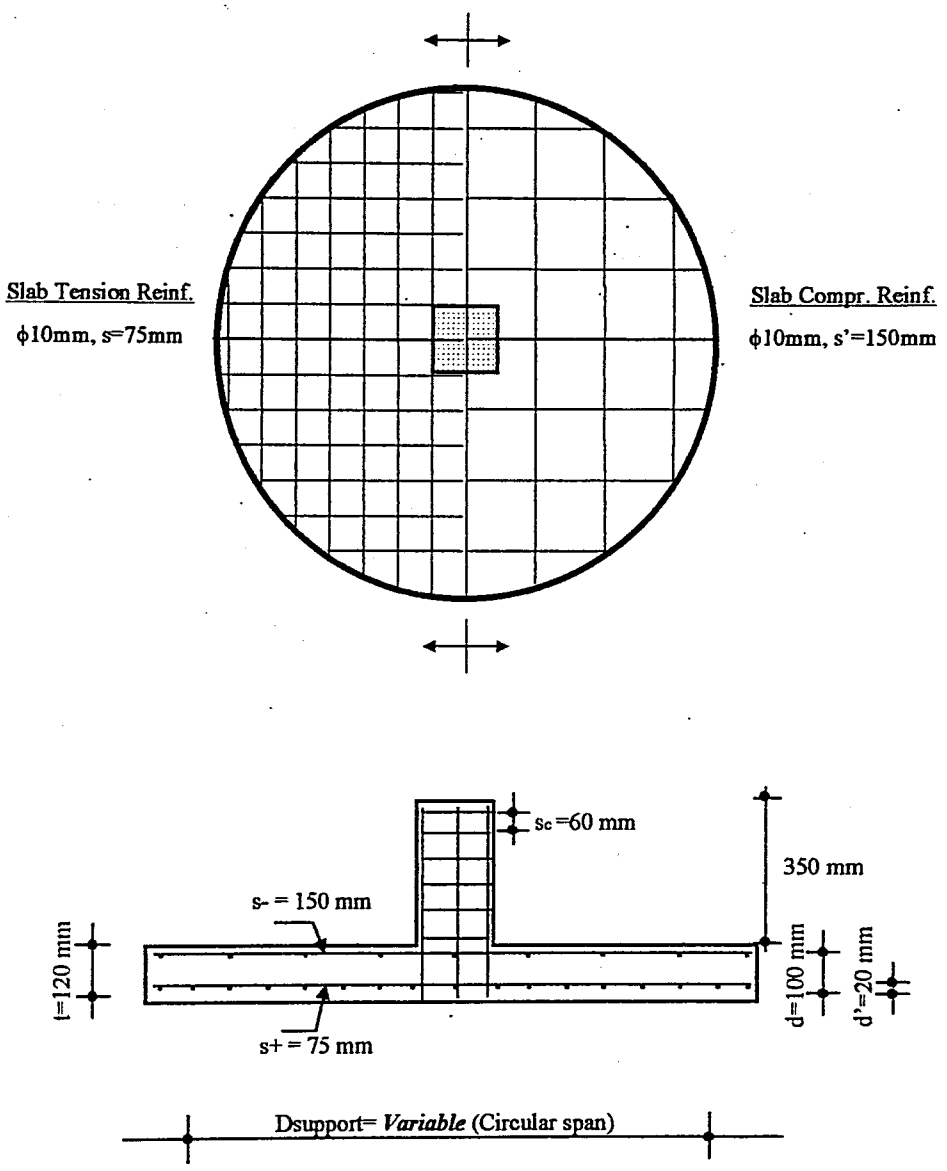

Figure 4.3. Slab reinforcement detail

4.3. Casting and Curing

Flat-plate test specimens were cast in the Structures Laboratory Testing Hall. Four wooden formworks were prepared for the specimens, each having different slab diameter and constant slab thickness (Figure 4.4). One piece steel ring formwork of t=120 mm was located on the wooden base and fixed with wooden wedges before the slab flexural reinforcement was laid into the formwork. In the mean time, the column longitudinal reinforcement together with the column confinement reinforcement was also located into the formwork. The slab flexural reinforcement mesh was seated on small wooden spacers in order to have a constant depth both for tensile and compressive reinforcement mash.

Column stub was cast using a laboratory mixed concrete after the slab concrete hardened for about a day. Twenty-two 150x300 mm concrete cylinder samples were cast from the slab concrete batch in order to follow the strength gain in the specimens. Both the specimens and the concrete cylinders were cured for three days under wet burlap covers and left to the atmospheric conditions of the testing hall afterwards.

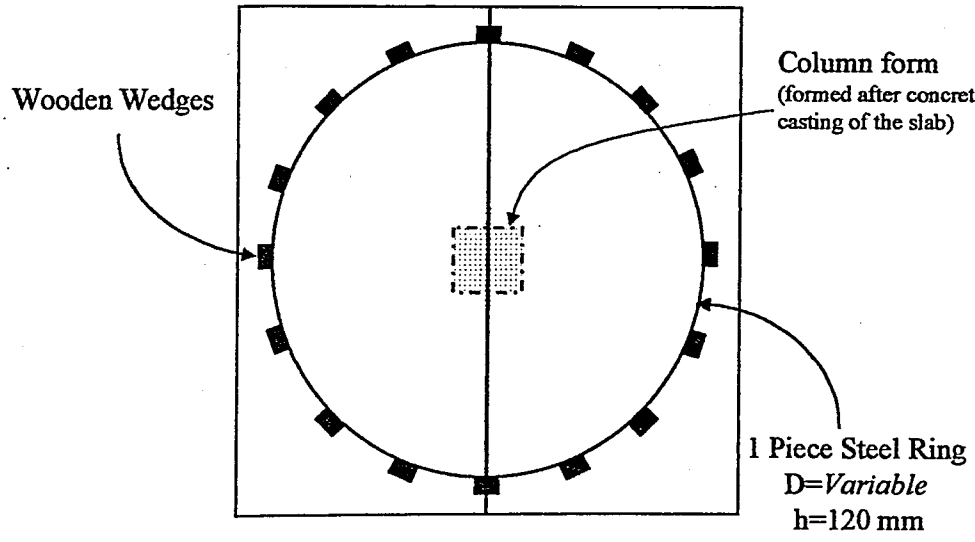

Figure 4.4. Formwork Layout

4.4. Test Set-Up

Four flat-plate circular specimens were tested on the same day, in order to minimize the concrete strength fluctuations, with the following procedure. Specimens were seated on sixteen spherical-supports in order not to transfer any bending stiffness to the plate edges. The supports were sat on 200x200x400 mm concrete pedestals, and the necessary space for instrumentation beneath the specimen was supplied (Figure 4.5). Loading was done by a manually driven hydraulic pump, and the level of load was measured by an electronic Load Cell. Thus the test was load controlled and the data was continuously fed to the Data Acquisition system. Semi spherical seat was located between the Load Cell and the column stub to insure the concentric application of the load. Three transducers were used for the displacement measurements. The slab out-of-plane deflection was measured right under the column stub and at two locations on the support perimeter (Figure 4.6).

Specimens were located under a steel loading frame available in the Structural Lab Testing Hall, on the strong floor. Before the specimens were seated, the concrete pedestals were aligned over a predetermined perimeter and levelled by using plaster capping. Roller supports on top of the concrete pedestals were also aligned and levelled for a uniform support perimeter. For the cases of loose contact between the roller supports and the slab, metal shims were used in between.

A heavy steel plate was located on the column stub for the even distribution of the applied load on the column. In each specimen, the load was applied to the centroid of the column stub cross-section.

Although the test set-up was stable against overturning and side-sways, each specimen was also hang loose by the laboratory crane in order to make the displacement transducers, which were below the specimen, safe throughout the testing. A view from the test set-up and a close-up from the support conditions are given in Figure 4.7 and Figure 4.8.

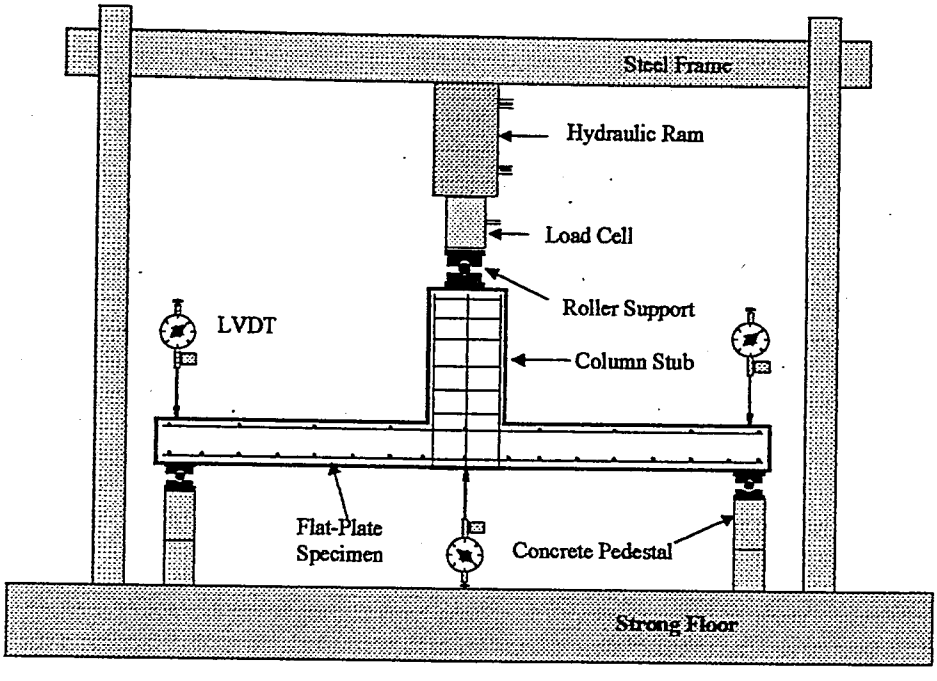

Figure 4.5. Schematic view of the test set-up

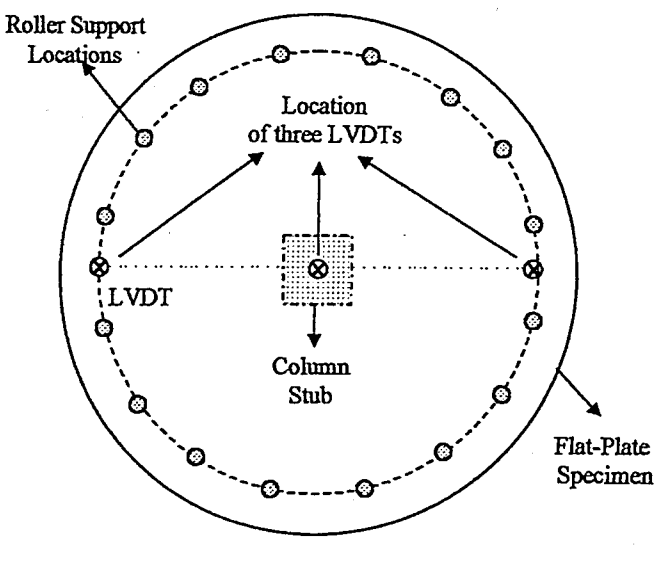

Figure 4.6. Location of displacement readings

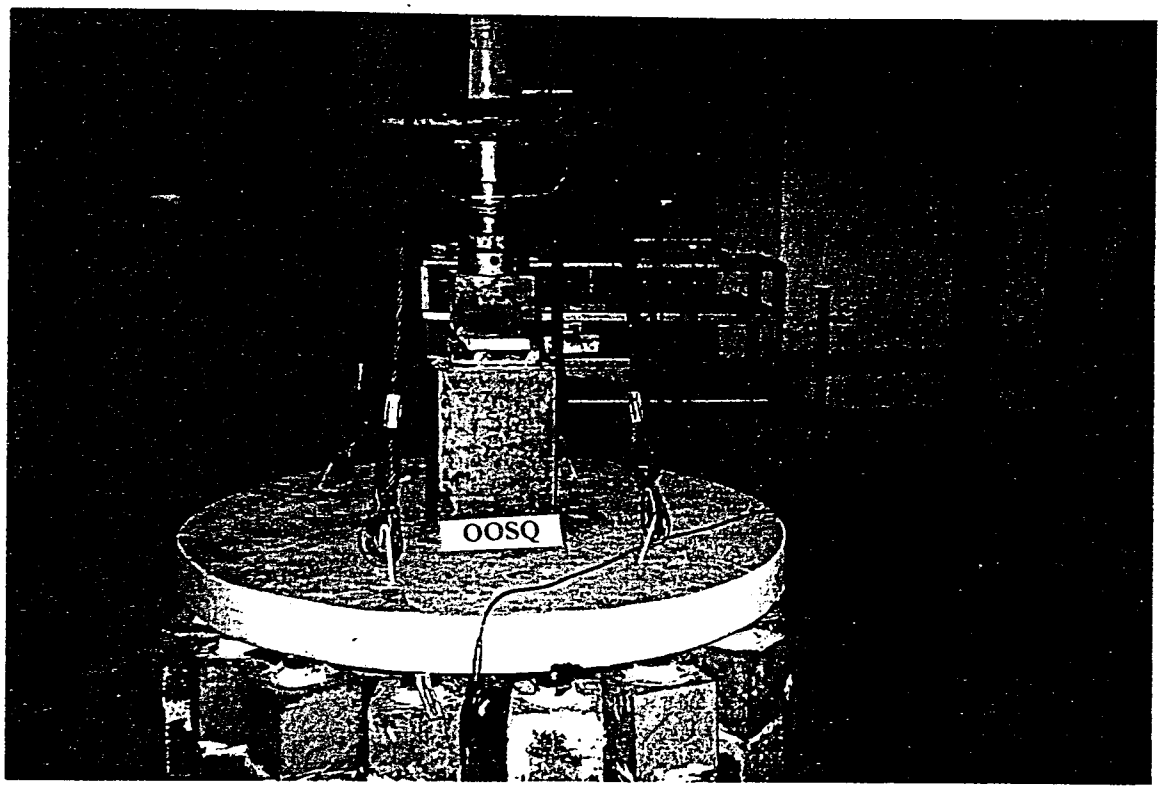

Figure 4.7. A view from the test set-up

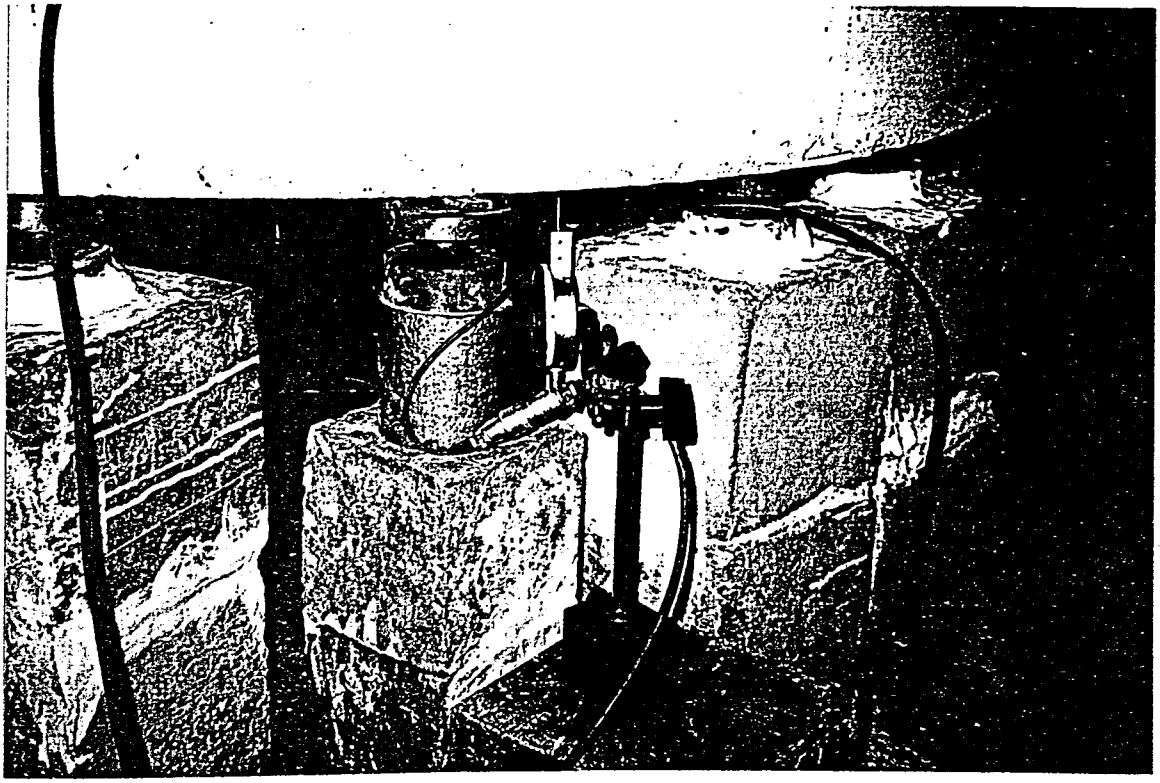

Figure 4.8. A close-up from the specimen supporting

5. TEST RESULTS

5.1. Material Tests

Material tests (compression test and split cylinder test) were performed on 150x300 mm concrete cylinders, which were cast from the same batch of specimens and underwent the same curing regime as the flat-plate specimens. 2000 kN capacity, servo valve controlled testing machine was used for both of the concrete tests. The Loading speed for compression tests was set to 0.2 MPa/second. Eight compression tests were done on the same day of structural testing and the results are given in Table 5.1. Sulphur capping on compression cylinders was made before the compression tests, in order to assure a uniform stress block on the cylinders. Four split cylinder tests were done under the same hydraulic testing machine with an added apparatus to the loading platens. The split cylinder tests are also given in Table 5.1.

Table 5.1. Concrete mechanical test results

Cylinder Test Number	150x300mm Concrete Cylinder Compressive Strength (MPa)	Average	150x300mm Concrete Cylinder Split Strength (MPa)
1	23.66	1	2.74
2	25.11	2	2.35
3	25.06	3	2.23
4	23.82	4	2.52
5	26.10	Average f_{sp}	2.46
6	24.75		
7	25.80		
8	24.58		
Average f_c'	24.86		

5.2. Load Deformation Behavior of Specimens

During the application of the load, the load deflection curve was traced on the electronic data acquisition screen, and the compression side of the flat plate was examined carefully for the possible existence of any cracking or crushing of concrete. The specimens were loaded well beyond their maximum load capacity in order to investigate the post-failure behavior. The loading was terminated when the traced load deflection curve started to raise at the residual load portion. Although the load was applied by a manually driven pump, it was tried to keep the loading speed constant among the test specimens.

Load readings in load-deflection curves are the values read directly from Load-Cell, while the center deflection values are the net center deflection calculated by using the readings from the deformation gauges located at the center and the perimeter of the flat plates. In the evaluation of the deflection values, the different slab support diameters (D_{sup}) need to be considered for a comparison between the specimens.

The experimental results of the flat-plate tests are given in Table 5.2, with reference to Figure 5.1. The flexural cracking load (P_{cr}) values were determined from the load deflection curves, instead of visual inspection during the loading, since the tension side of the flat-plates was not reachable due to the test set-up. Load level, at which the first change in the initial plate stiffness has been observed, was considered as the P_{cr} load, and the corresponding slab center vertical deflection values (δ_{cr}) are also given in Table 5.2.

The load, which is called the experimental punching capacity (P_p), was decided as the load level over which the load carrying capacity of the plate could not be increased. All specimens failed suddenly at P_p load level, indicating a brittle punching failure. The center deflection at the P_p load level (δ_p) and the slab center deflection values at successive 20 percents of the P_p load (δ_c) are given in Table 5.2 for all specimens.

The energy absorbed by the sub-assembly until failure can easily be calculated by assuming a linear variation in load deflection curves between the given δ_c values. In all of the test specimens, the load capacity of the flat-plates dropped suddenly beyond the failure

load, P_p. The drop in load was stabilized at a certain load level (P_{re}) and the specimens could carry this load under increasing slab center deflections. All the tests were terminated at a center deflection value (δ_{max}) around which the post failure load deflection curve started to raise again.

Load deflection curves and the deflection profiles of the specimens are given in Figure 5.2 to Figure 5.9. Loading in three of the flat plate specimens was in a monotonically increasing manner, and it was terminated well beyond the experimental failure point. On the other hand, an unintentional cyclic loading was performed on specimen OOSW, due to a wrong functioning in the hydraulic loading system. In the first cycle, the load reached approximately 75 percent of the experimental load capacity. Radial flexural cracks and the hairline cracks at approximately d/2 distance from the column stub on the flat plate on slab tension side was visible when the loading was terminated. In the second attempt for loading, all the load and displacement readings were initialized and it is given accordingly in Figure 5.6. The deflection profile values shown in Figure 5.7 are from the first loading until the crossing point of these two loading curves, and read from the second loading curve after this point.

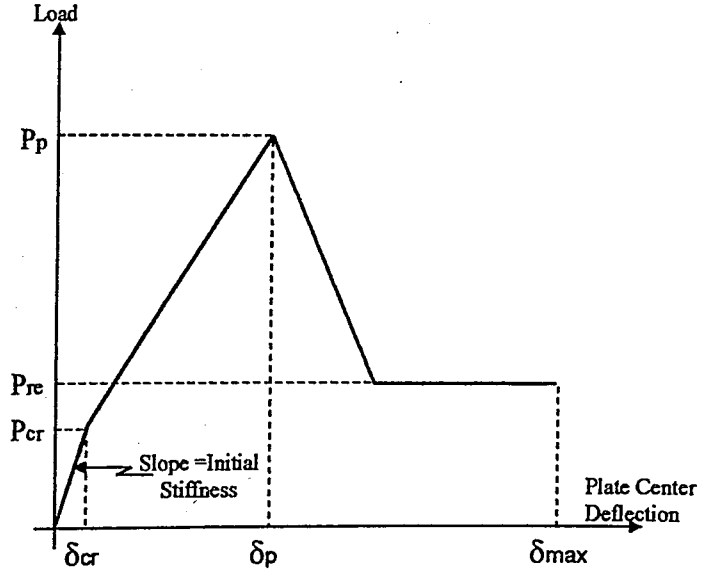

Figure 5.1. Idealized load-center deflection curve for test specimens

Table 5.2. Test results

Specimen		OOSQ	OORC	OOSW	OOTE
t (mm)		120	120	120	120
d (mm)		100	100	100	100
D_{sup} (mm)		1300	1480	1720	1464
r_{short}		300	120	120	120
r_{long}		300	480	720	463
s^+ (mm)		75	75	75	75
s^- (mm)		150	150	150	150
u_p (mm)		1600	1600	1600	1600
a/d		5	5	5	5
f_c' (MPa)		24.86	24.86	24.86	24.86
f_{sp} (MPa)		2.46	2.46	2.46	2.46
f_y (MPa)		547	547	547	547
P_p (kN)		353.60	327.81	359.49	347.03
δ_p (mm)		6.93	8.23	9.43	9.03
δ_c (mm)	@ 20% of P_p	0.34	0.35	0.53	0.52
	@ 40% of P_p	1.21	1.37	2.09	1.79
	@ 60% of P_p	2.82	3.33	4.60	3.85
	@ 80% of P_p	4.60	5.45	6.46	6.17
P_{cr} (kN)		113.35	108.55	108.85	109.53
δ_{cr} (mm)		0.68	0.79	1.08	0.85
P_{re} (kN)		144.44	123.45	151.70	135.03
δ_{max} (mm)		16.59	17.11	20.09	19.98
P_{TS} (kN)		279.21	279.21	279.21	279.21

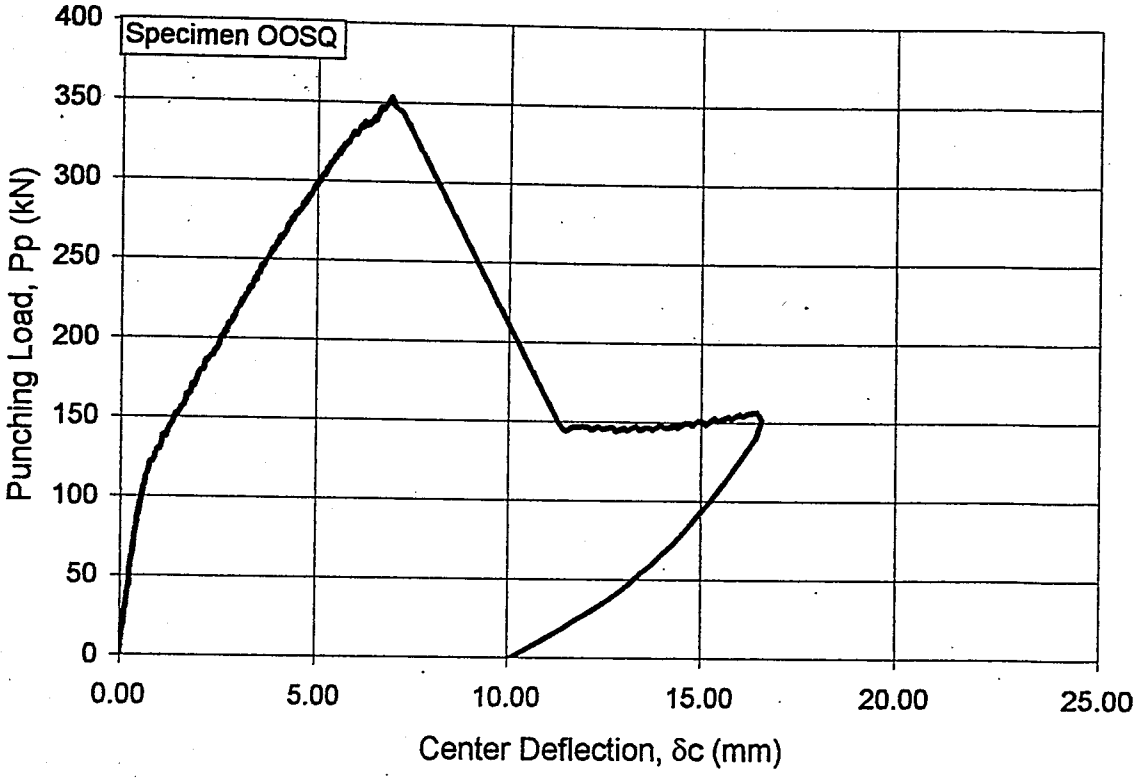

Figure 5.2. Load-center deflection curve of specimen OOSQ

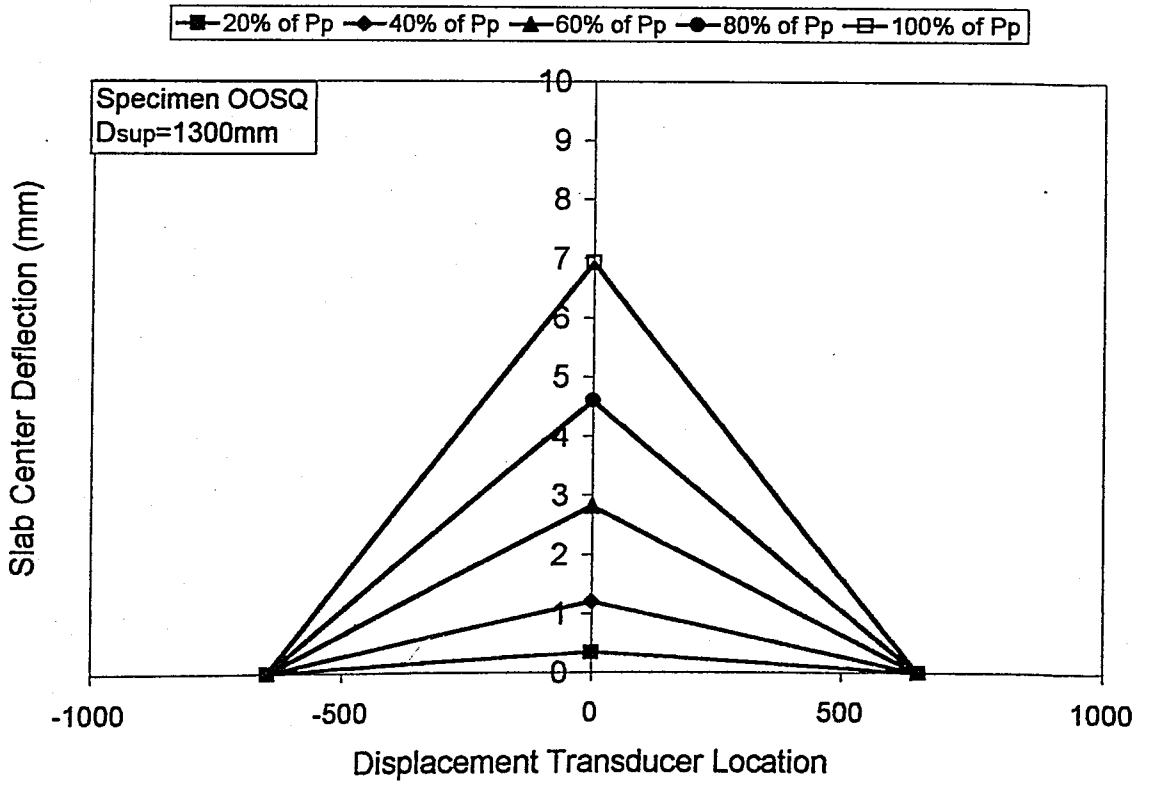

Figure 5.3. Slab center deflection profile of specimen OOSQ

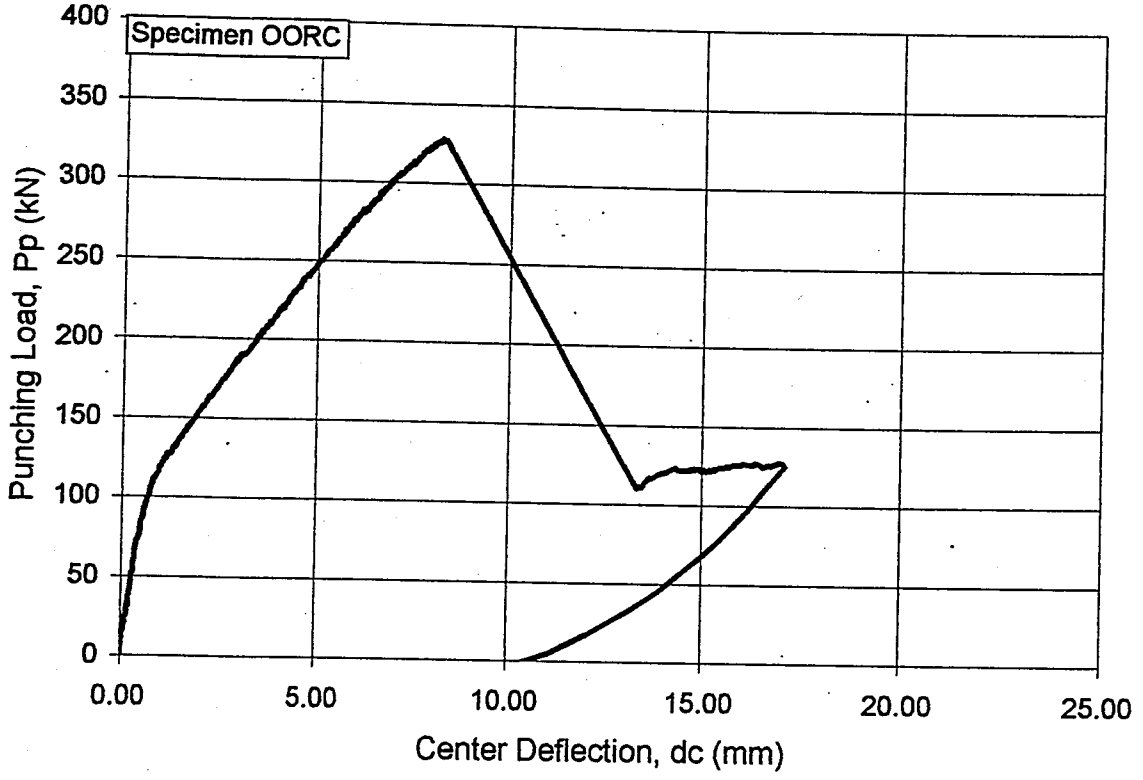

Figure 5.4. Load-center deflection curve of specimen OORC

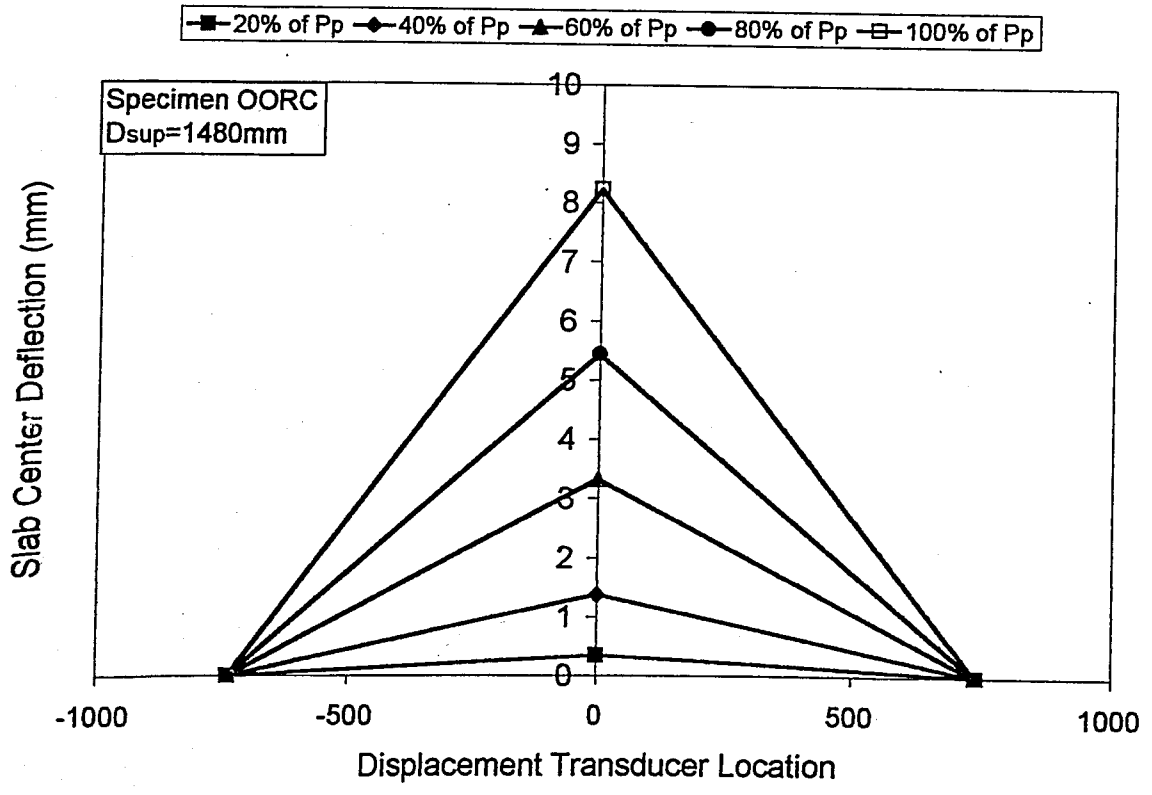

Figure 5.5. Slab center deflection profile of specimen OORC

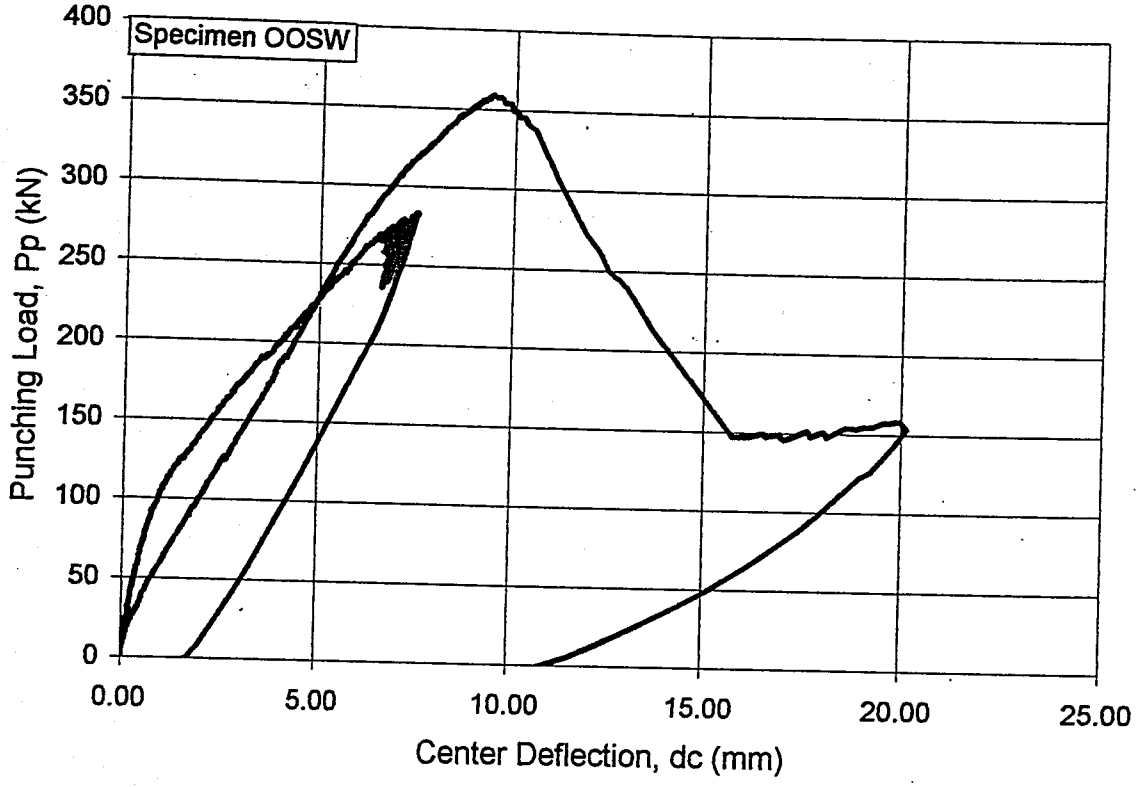

Figure 5.6. Load-center deflection curve of specimen OOSW

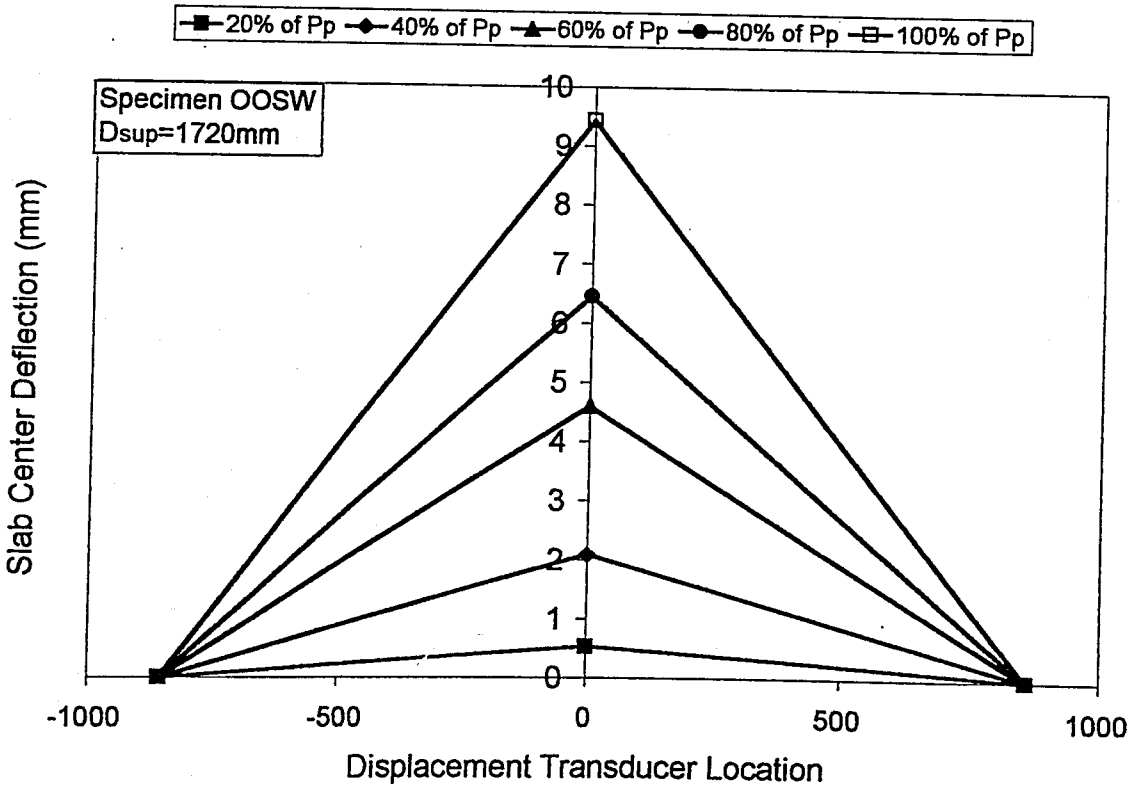

Figure 5.7. Slab center deflection profile of specimen OOSW

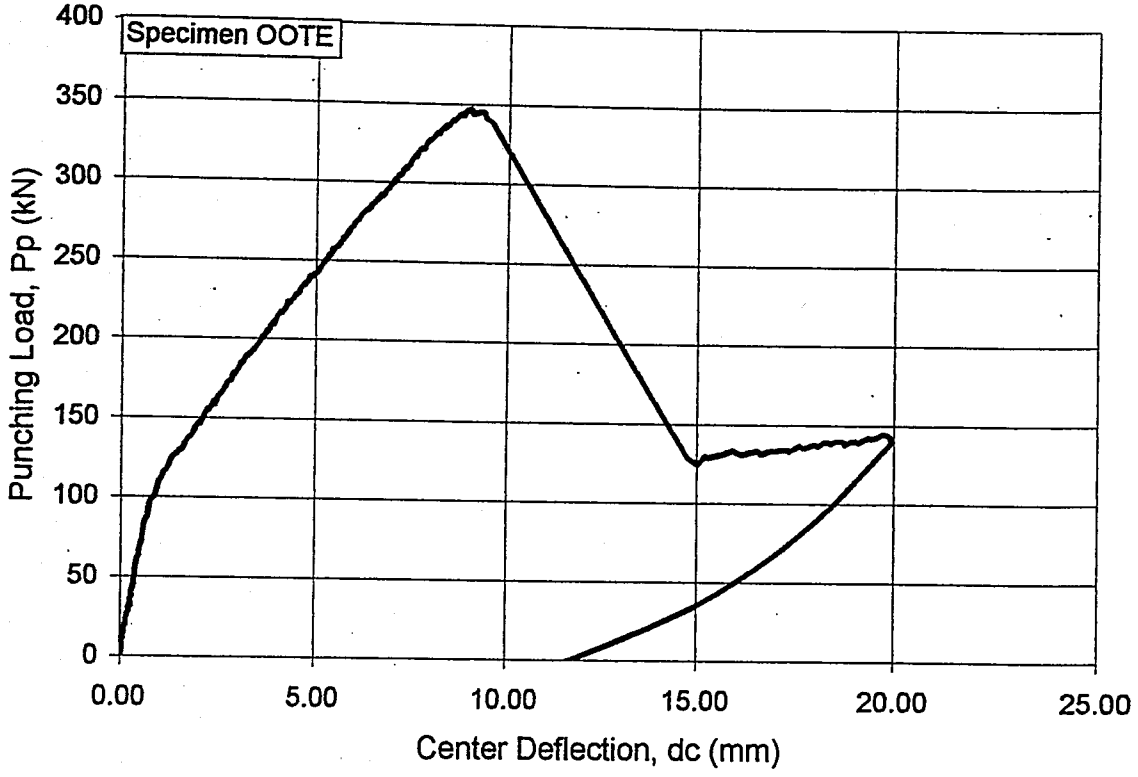

Figure 5.8. Load-center deflection curve of specimen OOTE

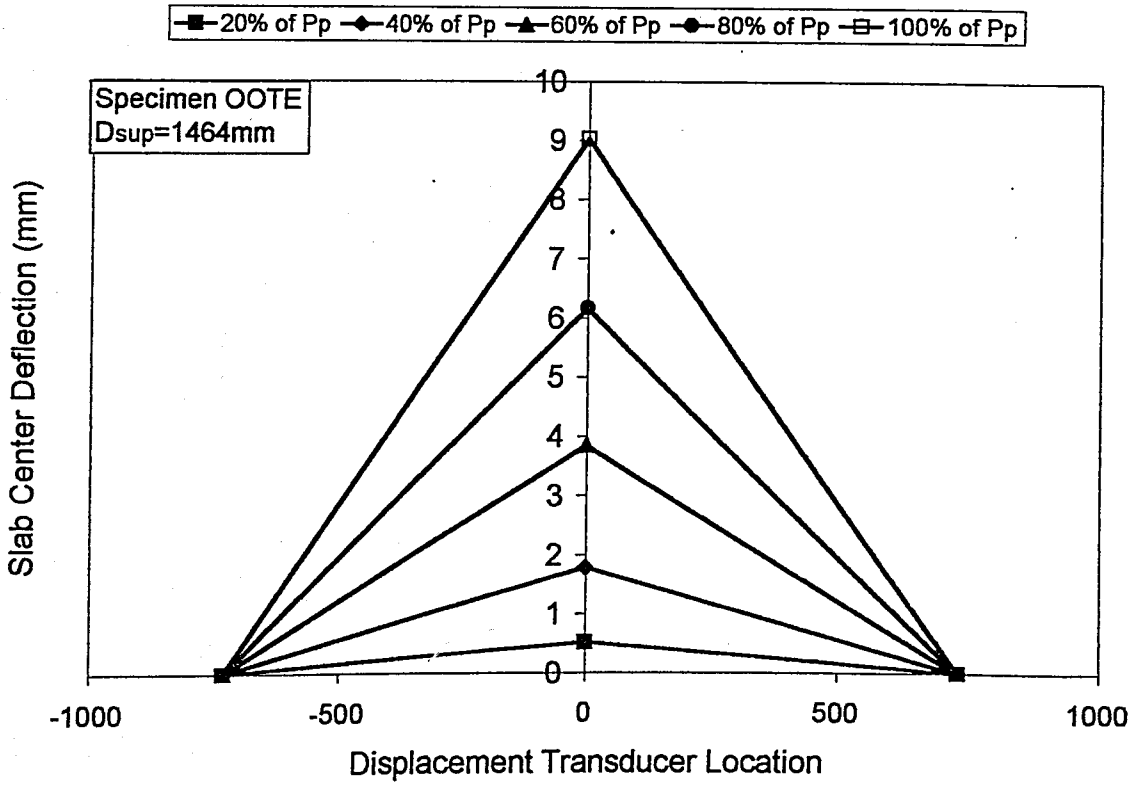

Figure 5.9. Slab center deflection profile of specimen OOTE

5.3. Cracking Behavior of the Test Specimens

The test set-up was such that, the compression side of the specimens was observable throughout the test, while the tension side of the specimens could only observed after the termination of loading due to the plate support conditions. Cracking or crushing type of plastic deformations on the compression side of the flat plate specimens was checked throughout the loading scheme of all specimens, while the crack map was observed, marked and photographed after the specimens were replaced to the storage hall from the test set-up. It needs to be clarified that the crack pattern observed and marked on the tension side of the specimens, are the cracks formed well beyond the experimental punching load, P_p.

Until the experimental failure load P_p, no crushing or cracking was observed on the plate compression side in either of the specimens. A sudden and brittle type of failure, resulting in a rapid drop in the load carrying capacity, took place when the column punched through the plate leaving a w=2-4 mm crack all around the column stubs. This type of crack was following the column perimeter in specimens OOSQ, OORC and OOSW. On the other hand the cracks on compression side of the specimen OOTE showed a different pattern with similar crack widths. In this specimen, cracks were following the edges and the outer corners of the T-shape, while a smooth curve of crack line was observed at the inner corners of the T-shape. The approximate perpendicular distance from the inner corner of the column stub to this crack was approximately 25 to 35 mm.

Tension side of the specimens could only be investigated between the supports with the help of a flashlight during loading. The first type of the cracks was the radial cracks starting from the column stub and traveling towards the support perimeter in all specimens. The crack width change with changing load levels throughout the test could not be traced. On the other hand, the crack map after the execution of the test was examined thoroughly. The crack patterns on the tension side of the specimens are shown in Figure 5.10 to Figure 5.17.

The crack patterns observed on the tension side of the specimens clearly revealed the column stub shape in every specimen.

The cracks, which led the specimens to the failure, were approximately located at a distance of 100 mm, which corresponds the flat plate effective depth. In all the specimens, the cracked portion of the slab, starting from the column stub edges, traced an approximately similar area.

Tension cracks on the specimen OOSQ compared to the rest of the specimens was less in intensity and in a much more circular form around the center of the column stub. This may be related to the relatively bigger column dimension to slab effective depth ratio. The crack intensity was high in OORC and OOSW specimens, especially on the region parallel to the smaller column dimension.

A uniform tension crack pattern was observed in specimen OORC relative to the specimen OOSW. Both radial and transverse cracking was observed in specimen OORC, on all sides of the column stub. On the other hand, radial and transverse cracks were observed only on the plate region parallel to the smaller column dimension of the OOSW specimen, and the cracking was mainly parallel to the column sides for the plate region parallel to the longer column dimension.

The tensile crack pattern in specimen OOTE clearly followed the column stub outer edges of the T-shape. Conversely, the crack formed on the inner edge region of the T-shape was on a contour approximately parallel to the line connecting the outer corners of the T-shape. As it is seen in Figure 5.16 and Figure 5.17, this contour is concave on one side and convex on the other side. Therefore, a clear evidence on the shape of this crack could not be obtained. For most practical purposes, the contour may be accepted as a straight line.

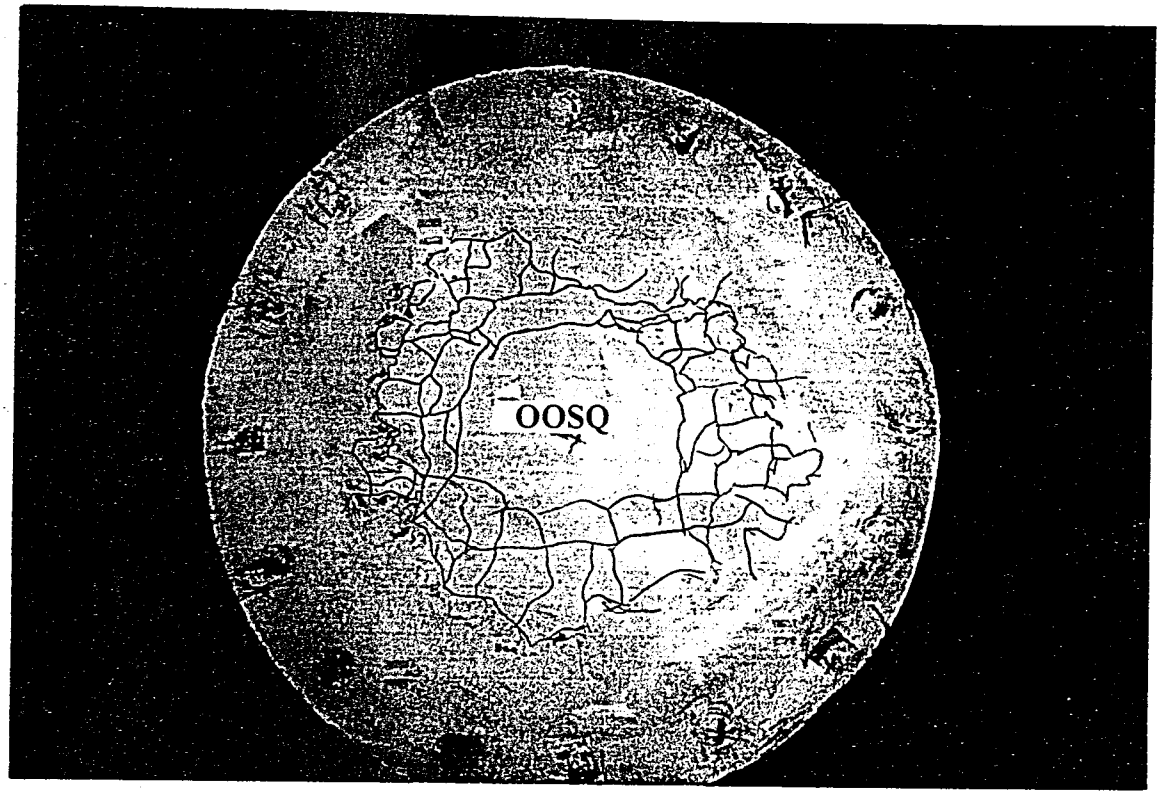

Figure 5.10. Crack pattern on tension side of specimen OOSQ

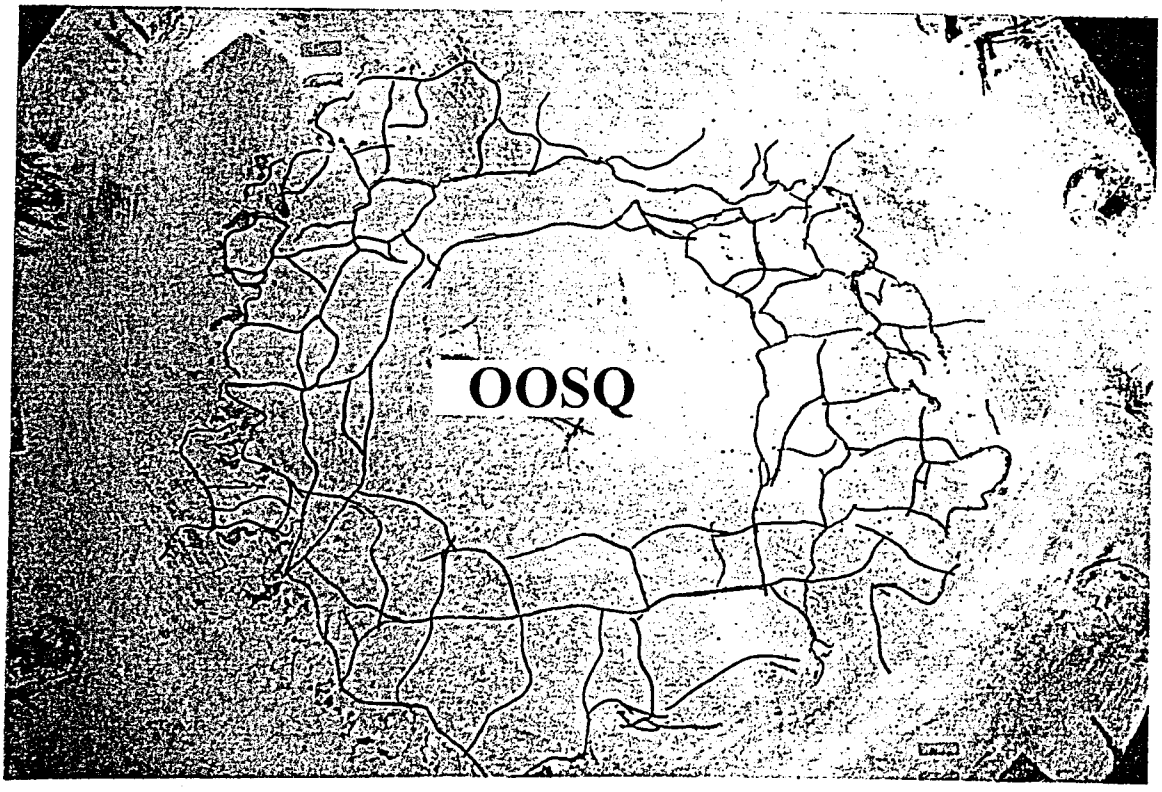

Figure 5.11. A close-up from specimen OOSQ crack pattern

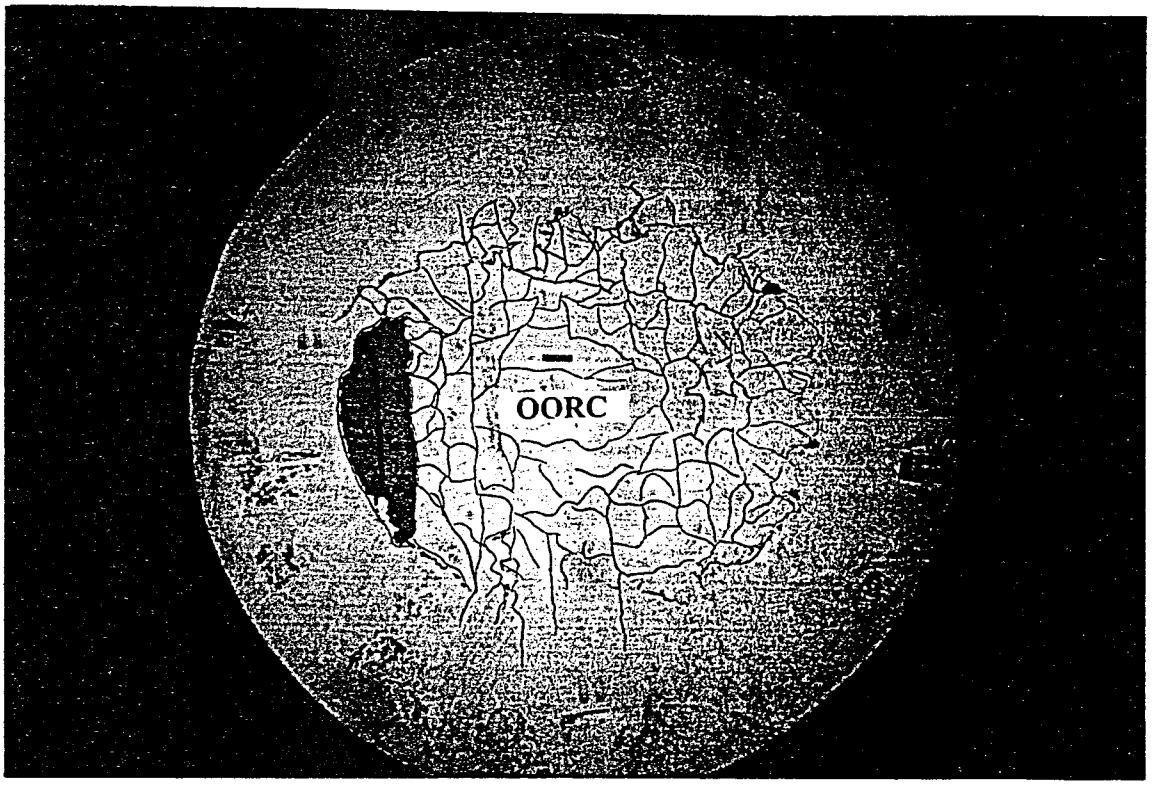

Figure 5.12. Crack pattern on tension side of specimen OORC

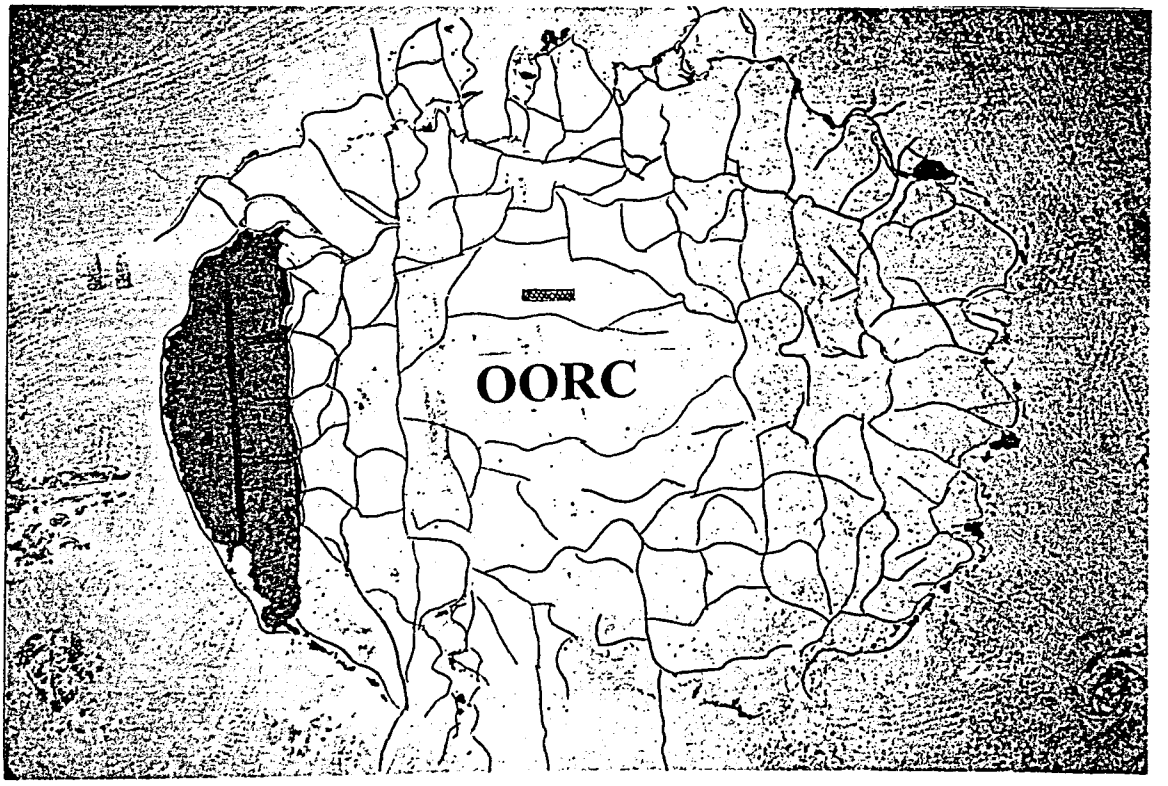

Figure 5.13. A close-up from specimen OORC crack pattern

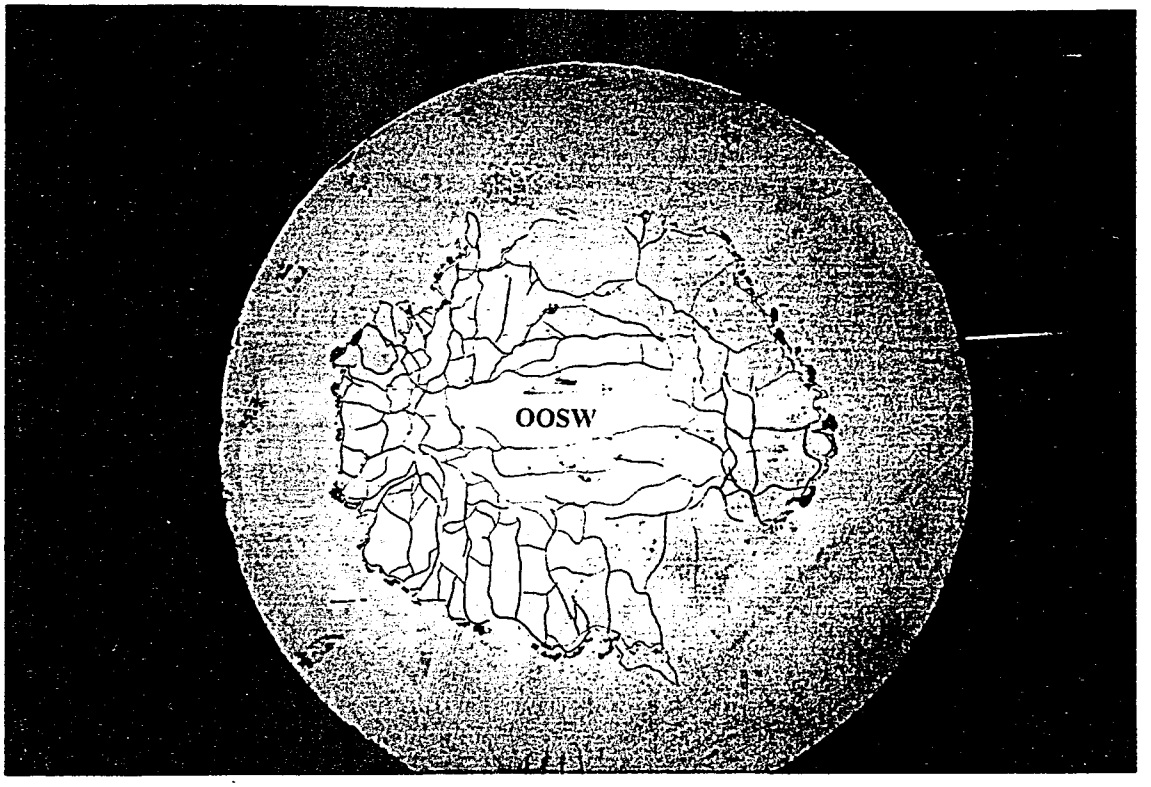

Figure 5.14. Crack pattern on tension side of specimen OOSW

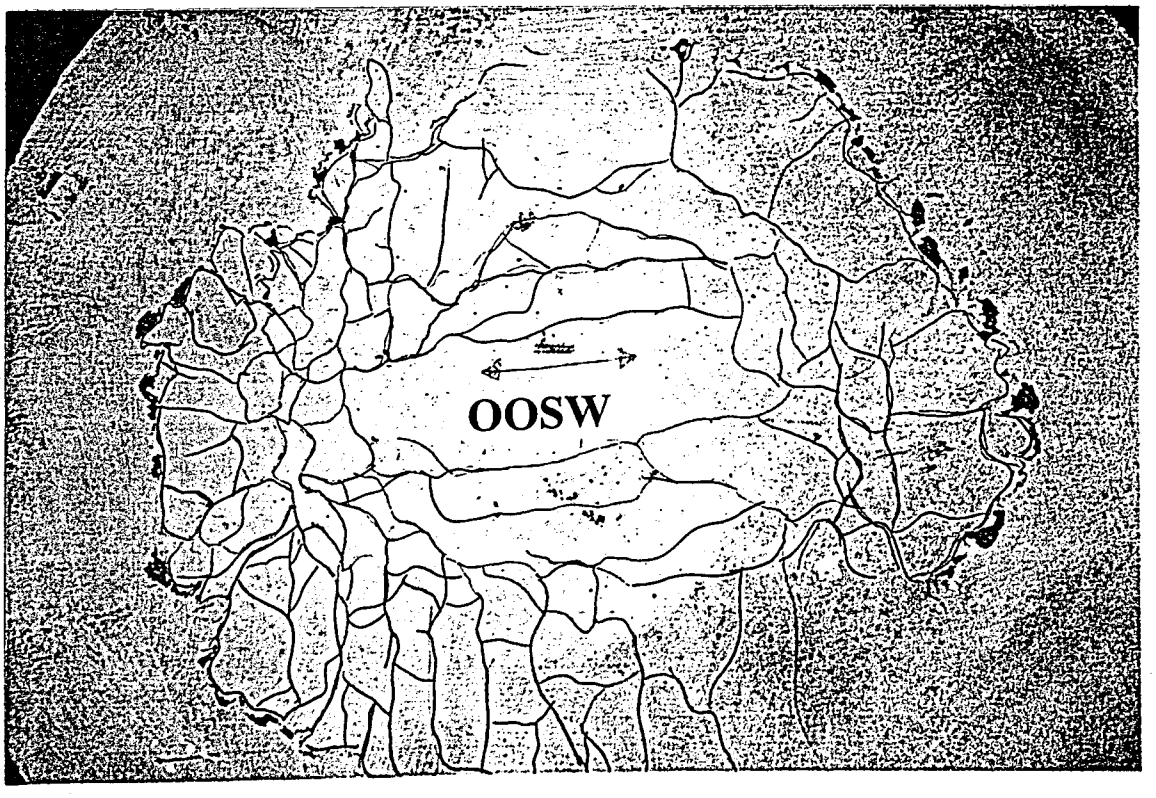

Figure 5.15. A close-up from specimen OOSW crack pattern

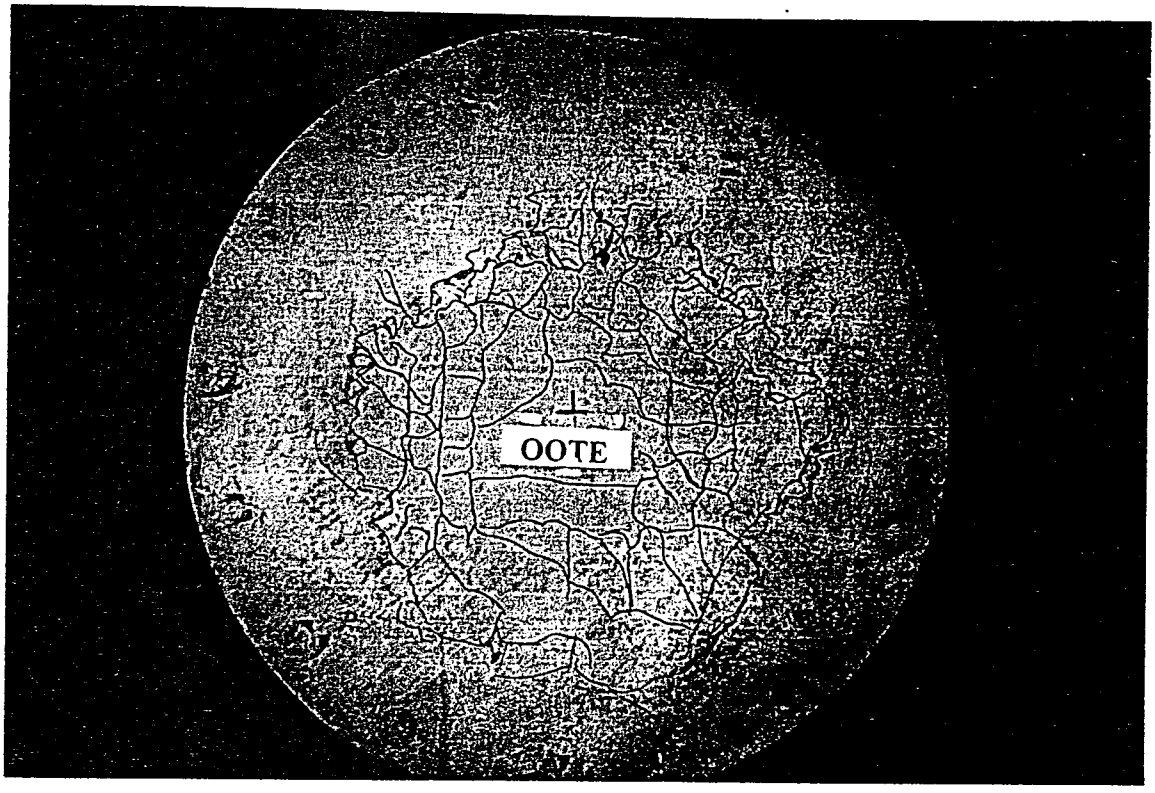

Figure 5.16. Crack pattern on tension side of specimen OOTE

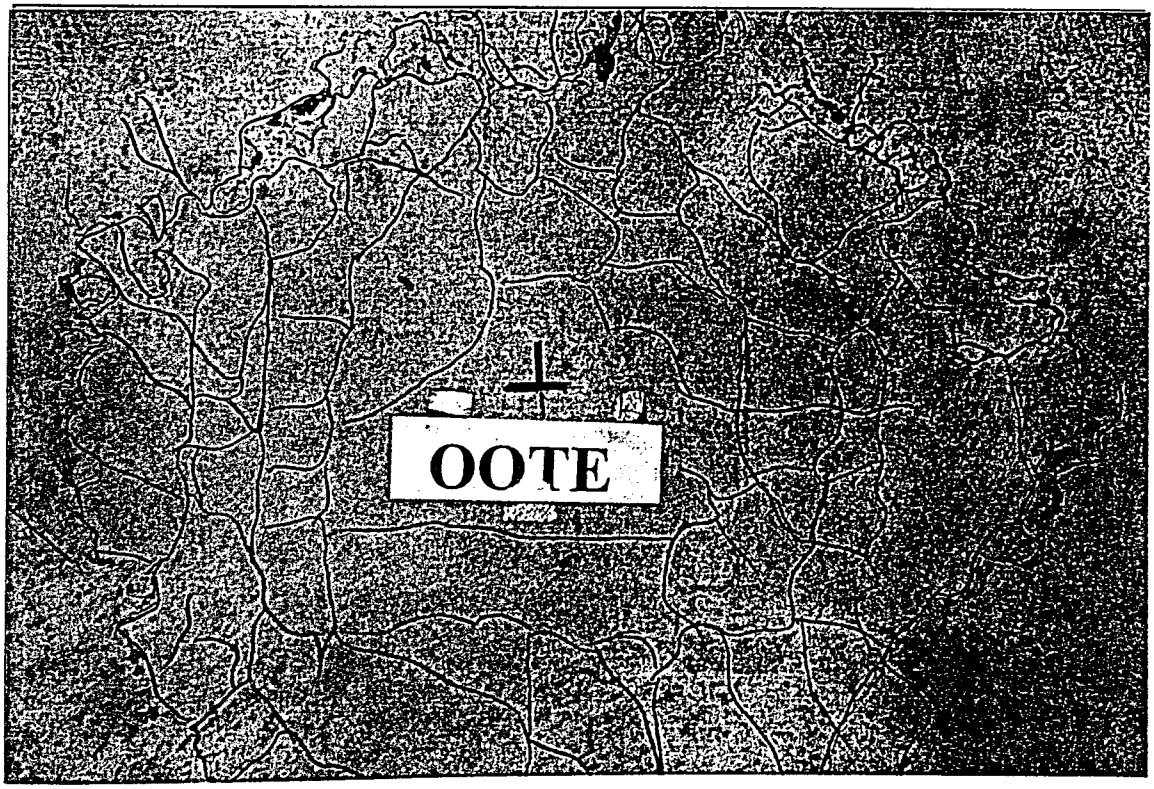

Figure 5.17. A close-up from specimen OOTE crack pattern

6. EVALUATION OF THE TEST RESULTS

The punching behavior and capacity of Normal Strength Concrete (NSC) flat plate systems with internal square columns under concentric loading was studied by other researchers, and the empirical equations derived from these studies are currently used in most of the national building design codes. When the column shape is highlighted in the previous available research, it may be concluded that, approximately threes quarter of the available data is on square columns and approximately only one-tenth of the available data is about shear wall punching.

Within the content of the current research, column stubs with aspect ratios changing from one (square column) to six (shear wall) was used in order to study the effect of column rectangularity on the capacity and behavior of the NSC flat plates under concentric loading. Mainly, the effect of column rectangularity on strength, deflections, energy absorption capacity and reliability of the TS-500 Building Design Code equations were studied and given below. Moreover, an attempt was made and discussed below to predict the shear stress at punching failure by considering the concrete strength, column rectangularity and the punching perimeter.

6.1. Effect of Column Rectangularity On Punching Strength

The punching failure may be defined as surpass of the principle tensile stresses beyond the tensile strength of the concrete itself over a perimeter, which is called the punching perimeter. For the case of square internal columns, there exist universally accepted methods to define the punching perimeters, and these are mostly verified by the experimental research. On the other hand, increasing column rectangularity may invoke some errors in the punching perimeter calculations. At this stage of the investigation, the punching perimeter calculation given in TS-500 [24] may need to be highlighted.

The theoretical punching perimeters for different shapes of internal rectangular columns according to TS-500 [24] are given in Figure 6.1.a-c. The punching perimeter for square, rectangular and T-shape columns is in the form of a closed perimeter as illustrated

in Figure 6.1a,c, and the perimeter length, u_{pTS} was calculated according to Equation 6.1. On the other hand, column rectangularity is considered for the shear walls as illustrated in Figure 6.1.b, and the perimeter length, u_{pTS} was calculated according to Equation 6.2.

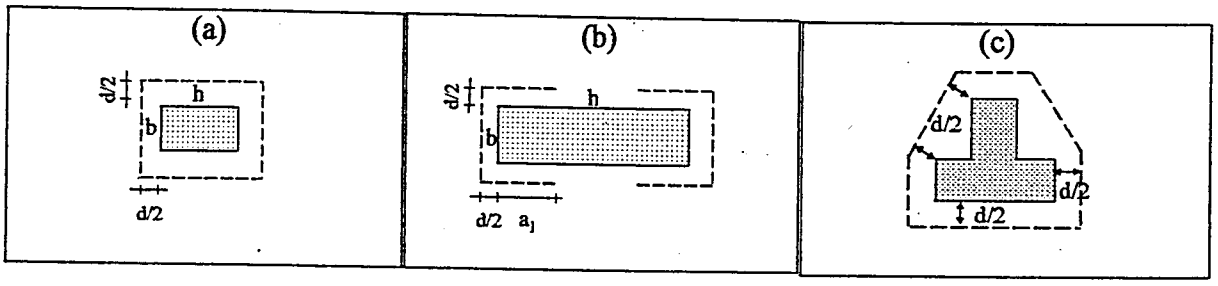

Figure 6.1. TS-500 [24] illustration of punching perimeter

$$u_{pTS} = 2*((b+d)+(h+d)) \tag{6.1}$$

$$u_{pTS} = 2*((b+d)+(2*a_1+d)) \tag{6.2}$$

The value a_1 of the perimeter, u_{pTS} in shear walls was calculated according to Equation 6.3.

$$a_1 = \text{smaller of} \begin{pmatrix} h/2 \\ 2*b \end{pmatrix} \tag{6.3}$$

The calculated theoretical punching perimeters and the shear stress over this perimeter at the time of punching failure are listed in Table 6.1. Experimentally obtained stresses at the time of punching failure, v_{cts} is calculated by dividing the punching load, P_p, by the product of the length of the punching perimeter, u_{pTS}, and the slab effective depth d, as given in Equation 6.4. The theoretical value for the stress level at the time of punching in TS-500, v_{TS}, is a function of concrete strength only and given in Equation 6.5.

$$v_{cts} = \frac{P_p}{u_{pTS}*d} \tag{6.4}$$

$$v_{TS} = 0.35 * \sqrt{f'_c} \tag{6.5}$$

Table 6.1. Comparison of the experimental and calculated strength capacities

Specimen	r_{short} (mm)	r_{long} (mm)	P_p (kN)	d (mm)	u_{pTS} (mm)	v_{cts} (MPa)	v_{TS} (MPa)	v_{cts}/v_{TS}
OOSQ	300	300	353.60	100	1600	2.21	1.75	1.27
OORC	120	480	327.81	100	1600	2.05	1.75	1.17
OOSW	120	720	353.49	100	1600	2.25	1.75	1.29
OOTE	120x170	463	347.03	100	1600	2.21	1.75	1.24

The punching strength of the specimens ranged between 2.05 MPa and 2.25 MPa, the highest being observed in shear wall type column stub specimen OOSW, and the lowest being observed in rectangular column stub specimen OORC.

The limited number of data of the current research revealed that the punching shear strength was inversely influenced by the increasing column aspect ratio until the limit of shear wall type of supporting members. Shear strength of the shear wall type of column stub member OOSW was nearly equal to that of the square column stub member OOSQ.

Although, a difference in punching shear strength between the specimens was observed, the calculated stress difference at the time of failure was within 10 percent for the batch of specimens. For the constant punching perimeter u_{pTS}=1600mm, the ratio of the experimental punching strength, v_{cts} to code given strength, v_{TS} was above unity in all specimens indicating a safety margin of approximately 25 percent in the code given values under concentric loading. T-shaped specimen, OOTE also revealed that the code approach of punching perimeter calculations yields safe results. Also, the observed punching perimeters of the tests are in good agreement with the code predictions.

6.2. Deflection and Stiffness Comparisons

Specimens tested in this research had different column dimensions and aspect ratios. In order to have a constant shear span to depth ratio (a/d), where the shear span is

defined as the minimum distance from the column stub to the support perimeter, different slab diameters were used for the test specimens. Therefore, the slab center deflections of the specimens may not be compared directly. The center deflection of a flexural member is directly proportional to the specimen span as given in Equation 6.6.

$$\delta_c = \frac{P L^3}{c E I} \tag{6.6}$$

Although, flexural stiffness (EI) also has a bearing on the deflection values obtained, for the most practical purposes, flexural stiffness was considered to be the same at any corresponding load stage among the specimens. The deflection values of the specimens may be corrected (normalized) for a slab of diameter D_{sup}=1500 mm as shown in Equation 6.7. The value of D_{sup}=1500 mm was chosen arbitrarily.

$$\delta_c^* = \frac{1500^3}{L^3}\delta_c \tag{6.7}$$

Load deflection curves of all the specimens are given in Figure 6.2 for comparison purposes. In this graph, the center deflection values are the net values obtained directly from data acquisition system, and from here on it is going to be referred as raw displacement data within this heading. On the other hand, the load deflection curves with corrected center deflection readings according to the Equation 6.7 are given in Figure 6.3.

It was observed both from the raw data and the corrected data that, the slope of the falling branches of the specimens, had similar tangent stiffness values. Specimen OOSQ yielded the highest initial and tangent stiffness values in the raw data graphs. Other three specimens had practically similar values in Figure 6.2. On the other hand, the tangent and secant stiffness values of OOSW yielded the highest values with corrected displacements.

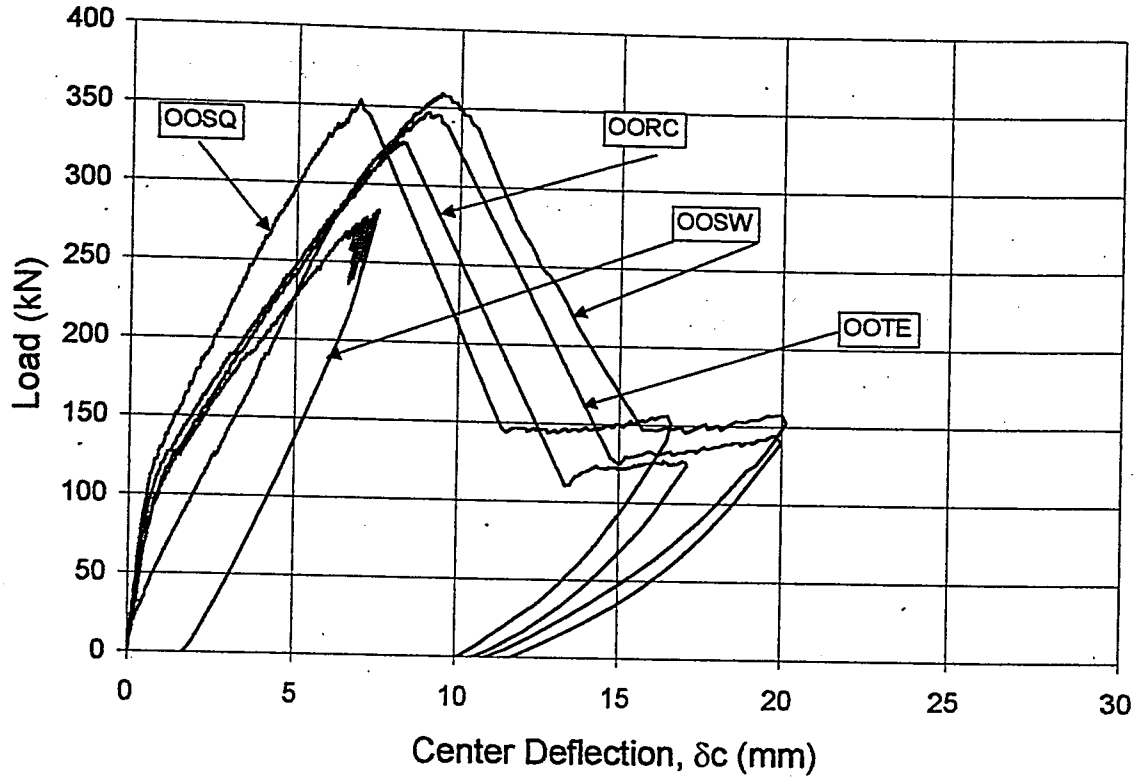

Figure 6.2. Comparison of the load-deformation curves

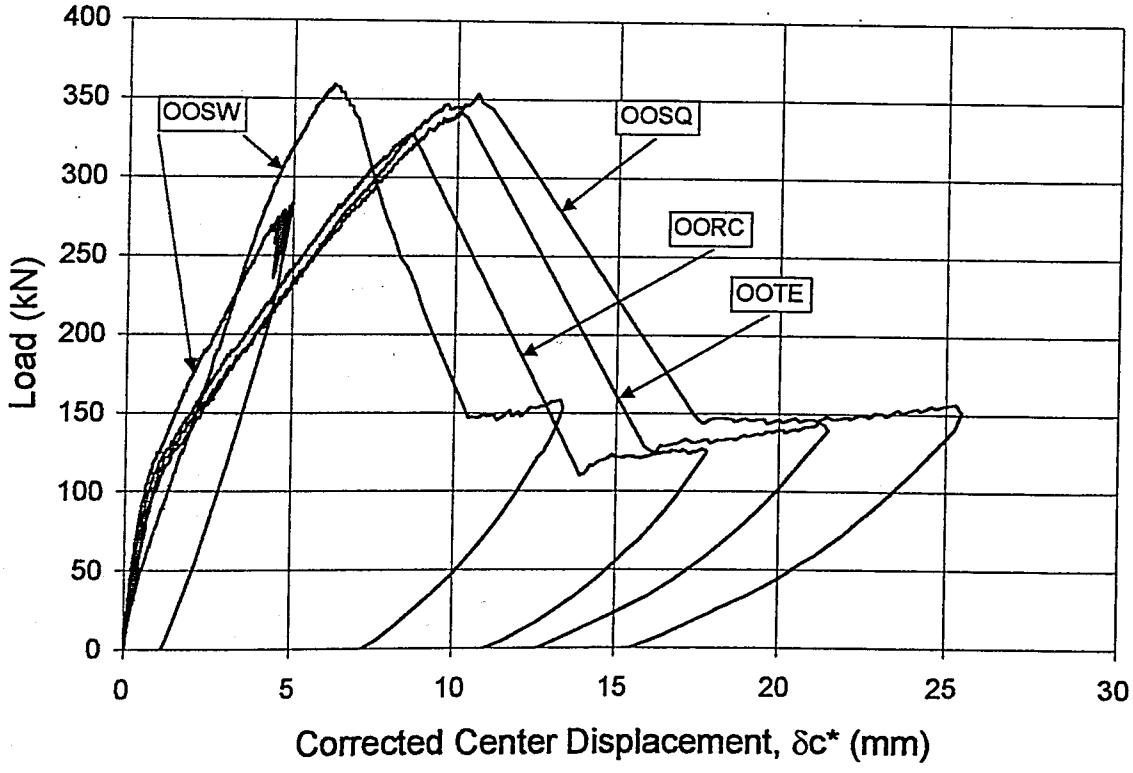

Figure 6.3. Comparison of the load-corrected deformation curves

Initial stiffness of the specimens with the raw data (K_i) was calculated by using Equation 6.8, while the initial stiffness using the corrected values (K_i^*) were calculated according to Equation 6.9.

$$K_i = \frac{P_{cr}}{\delta_{cr}} \tag{6.8}$$

$$K_i^* = \frac{P_{cr}}{\delta_{cr}^*} \tag{6.9}$$

Similarly, the tangent stiffness (K_t) and the tangent stiffness by using the corrected displacements (K_t^*) were calculated according to the Equation 6.10 and Equation 6.11 respectively. In these equations, it was assumed that the tangent stiffness between the load level of initial flexural cracking and the failure of the flat plate was not changing.

$$K_t = \frac{P_p - P_{cr}}{\delta_p - \delta_{cr}} \tag{6.10}$$

$$K_t^* = \frac{P_p - P_{cr}}{\delta_p^* - \delta_{cr}^*} \tag{6.11}$$

In some of the analytical approaches, the secant stiffness of the sub-assembly may be used. As it was defined before, secant stiffness was also calculated for the raw data (K_{sc}) and for the corrected deflections (K_{sc}^*) with Equation 6.12 and Equation 6.13, respectively. The calculated stiffnesses using the raw and corrected deflection values are given in Table 6.2.

$$K_{sc} = \frac{P_p}{\delta_p} \tag{6.12}$$

$$K_{sc}^* = \frac{P_p}{\delta_p^*} \tag{6.13}$$

Table 6.2. Center displacements and stiffness values of specimens

Specimen		OOSQ	OORC	OOSW	OOTE
P_p	(kN)	353.60	327.81	359.49	347.03
P_{cr}	(kN)	113.35	108.55	108.85	109.53
δ_p	(mm)	6.93	8.23	9.43	9.03
δ_{cr}	(mm)	0.68	0.79	1.08	0.85
D_{supp}	(mm)	1,300	1,480	1,720	1,464
δ_p^*	(mm)	10.64	8.57	6.26	9.71
δ_{cr}^*	(mm)	1.04	0.82	0.72	0.91
K_i	(N/mm)	166,691	137,405	100,787	128,859
K_i^*	(N/mm)	108,468	132,055	152,025	119,835
K_t	(N/mm)	38,440	29,470	30,016	29,034
K_t^*	(N/mm)	25,018	28,306	45,250	26,992
K_{sc}	(N/mm)	51,025	39,831	38,122	38,431
K_{sc}^*	(N/mm)	33,208	38,259	57,472	35,728
K_t/K_i		0.23	0.22	0.29	0.23
K_t^*/K_i^*		0.23	0.22	0.29	0.23
K_{sc}/K_i		0.31	0.29	0.38	0.30
K_{sc}^*/K_i^*		0.31	0.29	0.38	0.30

The change in stiffness values after cracking was observed to be very high, resulting in a tangent stiffness, which equals approximately 24 percent of the initial stiffness. When the corrected displacement values were used, the ratio remained approximately same. Beside this, the secant stiffness values were approximately 32 percent of the initial stiffness regardless of the use of raw or corrected displacement values.

The three stiffness values, namely initial, tangent and secant stiffness for the specimens may be considered to be similar with their counterpart corrected values for most practical purposes for specimens OORC and OOTE. On the other hand, the change in stiffness values may not be ignored for the specimens OOSQ and OOSW depending on whether the raw or corrected displacements are used.

6.3. Energy Absorption of Test Specimens

It was observed that the shape of the load deflection curves differed from each other due to the differences in column stub shape and aspect ratio as well as the differences in slab support diameter, D_{sup} although the shear span to depth ratio, a/d was constant for all the specimens. These differences may also influence the energy absorption rate of the specimens.

The energy absorbed until the load level of punching failure P_p, was calculated for all the specimens, and this value was called E_t under this heading. The E_t values differed from each other due to the variables of the current investigation. Instead of comparing the E_t values among specimens, the rate of energy absorption for each specimen was attempted to discuss. At successive steps of 20 percent increases of corresponding P_p values, the absorbed energy, E_{20} was calculated and the ratio of E_{20} to E_t was given in Table 6.3.

Table 6.3. Ratio of the absorbed energy by the specimens

Load Level	E_{20} / E_t			
% of P_p	OOSQ	OORC	OOSW	OOTE
0% to 20%	0.01	0.01	0.01	0.01
20% to 40%	0.06	0.06	0.09	0.07
40% to 60 %	0.18	0.18	0.22	0.18
60% to 80%	0.28	0.28	0.23	0.28
80% to 100%	0.47	0.47	0.46	0.45

The E_{20}/E_t values of the specimens are plotted in Figure 6.4 for the purpose of comparison. It may be concluded that, nearly all the specimens have similar energy absorption rate with respect to their own E_t values regardless of the variables of the current experimental investigation.

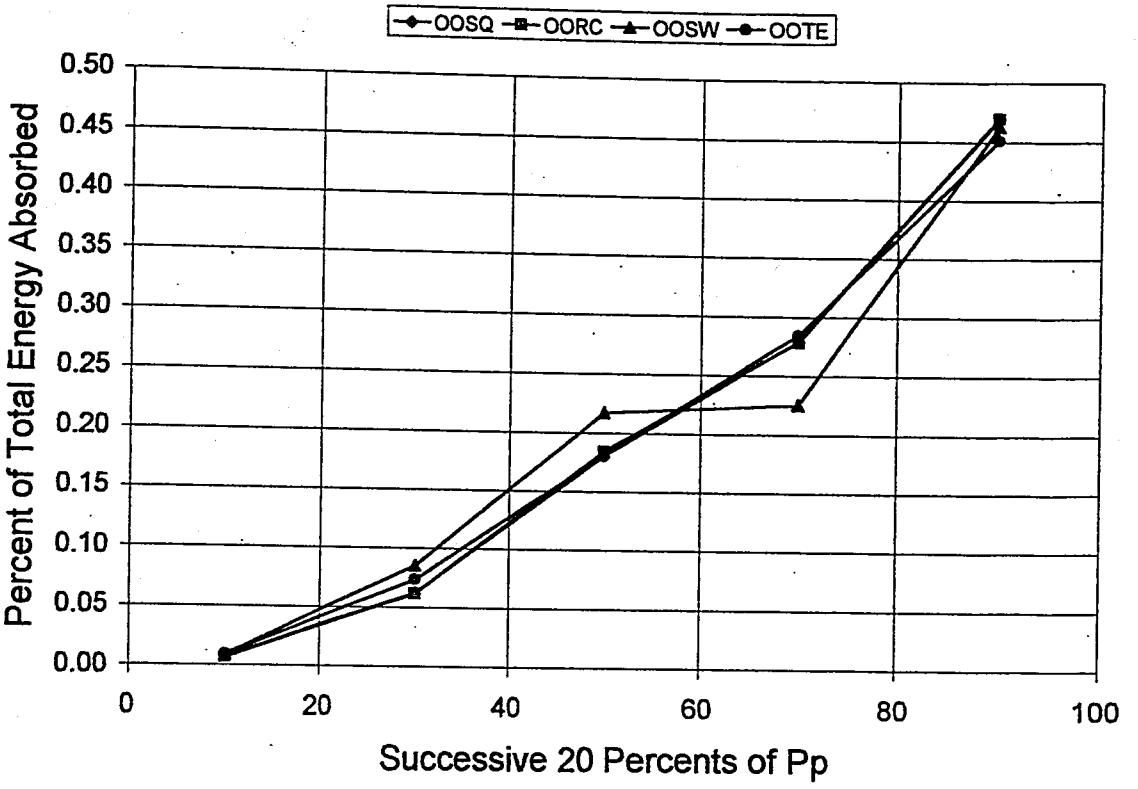

Figure 6.4. Absorbed energy curve at 20 percent intervals of P_p

6.4 Residual Load Capacities of the Specimens

The former Bogazici tests [9, 18] on the punching behavior of the flat plates revealed that the slabs with internal column stubs of square cross section had a residual load capacity beyond the punching failure load level, related to the concrete compressive strength, slab reinforcement ratio, existence of steel fiber reinforcement, and the load eccentricity. This residual load capacity was reported both under eccentric-monotonic loading [9], and eccentric-reversed-cyclic loading [18].

In the current research, the load capacity of all the specimens dropped suddenly beyond the failure load, P_p. Beyond the δ_p displacement value, the drop in load was stabilized at a certain load level, P_{re} and the specimens could carry this load under increasing slab center deflections. The residual loads of the current investigation were influenced by the column stub shape and aspect ratio. The experimental residual load

levels of the specimens and the predictions of the capacities by Ozden's equations [9] are given in Table 6.4.

Although, the specimens are considered as failed beyond P_p, the residual load capacity, P_{re} has prime importance in the nonlinear capacity predictions in push-over analysis of the flat plate structures. The P_{re} load capacity may also be used in determining the redistribution of loads in the flat plate systems with multiple columns, in progressive failure analysis of such structures.

The equations derived from the previous Bogazici research data [9] utilizes the total slab reinforcement cross section passing through the punching perimeter (ΣA_s, mm^2); yield strength of the slab reinforcement (f_y, MPa); load eccentricity factor (γ, without unit); concrete cylinder compressive strength (f_c', MPa); and the flexural capacity of unit width of slab (m, kN.m/m), for the calculation of the residual load capacity of the failed flat plates. Two equations were derived and reported by Ozden [9] for the P_{re} capacity calculations and they are given in Equation 6.14 and Equation 6.15. Either of the equations are reported to be useable, the second being more reliable.

$$P_{re}^{c1} = \frac{45 * \sum A_s}{1000} \quad \text{(kN)} \tag{6.14}$$

$$P_{re}^{c2} = 1.15 \frac{\sum A_s * f_y * \gamma * \sqrt{f_c'}}{1000 * m} \quad \text{(kN)} \tag{6.15}$$

In both of the above equations, the column rectangularity is not being considered explicitly, instead the ΣA_s is calculated accordingly, since the data from which the above equations were derived contained only square internal columns.

The total slab reinforcement cross sectional area passing through the punching perimeter was calculated by two different approaches. In the first approach, the theoretical punching perimeter specified in TS-500 [24] was used and the corresponding steel area ΣA_{s1} was obtained. In the second approach, especially for specimen OOSW, the punching perimeter was considered as continuous and a different steel area (ΣA_{s2}) was obtained.

Table 6.4. Experimental and calculated residual load capacities

(1)	Specimen		OOSQ	OORC	OOSW	OOTE
(2)	P_{re}	(kN)	144.44	123.45	151.70	135.03
(3)	f_c'	(MPa)	24.86	24.86	24.86	24.86
(4)	f_y	(MPa)	547.00	547.00	547.00	547.00
(5)	m	(kN.m/m)	50.31	50.31	50.31	50.31
(6)	γ	-	1.00	1.00	1.00	1.00
(7)	ΣA_{s1}	(mm^2)	2496.00	2184.00	2496.00	3120.00
(8)	ΣA_{s2}	(mm^2)	2496.00	2184.00	3432.00	3120.00
(9)	P_{re}^{c1} with ΣA_{s1}	(kN)	112.32	98.28	112.32	140.40
(10)	P_{re}^{c1} with ΣA_{s2}	(kN)	112.32	98.28	154.44	140.40
(11)	P_{re}^{c2} with ΣA_{s1}	(kN)	155.61	136.16	155.61	194.51
(12)	P_{re}^{c2} with ΣA_{s2}	(kN)	155.61	136.16	213.96	194.51
(13)	(2) / (9)	-	1.29	1.26	1.35	0.96
(14)	(2) / (10)	-	1.29	1.26	0.98	0.96
(15)	(2) / (11)	-	0.93	0.91	0.97	0.69
(16)	(2) / (12)	-	0.93	0.91	0.71	0.69

The residual load capacity predictions, as shown in Table 6.4 has good agreement with the experimental data of the current investigation. Equation 6.14 predictions have a higher safety margin, while the Equation 6.15 is more precise for the test specimens excluding the T-shaped specimen OOTE. The error in OOTE capacity prediction may be invoked by the existence of the inclined punching perimeter in plan with respect to the slab reinforcement grids.

6.5. Evaluation of Available Data in Literature

The available test data in the literature is filtered for the Normal Strength Concrete flat plates with square and rectangular internal column stubs loaded concentrically, where the slabs contain no holes, and the specimens are listed in Table 6.5. The forty-four specimens satisfying the constraints listed above are sorted primarily according to the

column aspect ratio and secondarily with respect to the r_{long}/d ratio in Table 6.4. Specimens of the current experimental investigation are also included in this table. Dimensional, material, reinforcement layout and failure loads are listed together with the names and the reference numbers of the published papers.

Due to the column aspect ratios and slab depths, some of the specimens may have discontinuous calculated punching perimeters, u_{pTS} as defined in TS-500 [24] and given in Equation 6.2. The crack patterns given in Chapter 5 yield that, the punching perimeter of the shear wall type column stubs may not be discontinuous but continuous at a distance d/2 from the column stubs. For this reason a new continuous punching perimeter, u_{pc} is defined as given in Equation 6.16 with reference to Figure 6.1.

$$u_{pc} = 2*((b+d)+(h+d)) \tag{6.16}$$

In this equation it is assumed that, the punching perimeter of a rectangular column lies at a distance of d/2 from the column stub and it is continuous over this perimeter, regardless of the column aspect ratios. The shear stress over this perimeter at the time of punching failure, v_{ce} may be calculated as given in Equation 6.17.

$$v_{ce} = \frac{P_p}{u_{pc} * d} \tag{6.17}$$

The above approaches are for determining the shear strength achieved at the flat-plate-to-column sub-assemblies in the experimental investigations. Beside this, a method need to be developed in order to achieve this experimental value from the givens of the sub-assemblies. It was reported that [9], the punching shear strength of flat plates may be calculated simply by considering the r_{long}/d ratio of the column stub and the concrete strength, f_c' as given in Equation 6.18.

$$v_{cl} = 0.7 * \sqrt{\frac{f_c'}{r_{long}/d}} \tag{6.18}$$

The Equation 6.18 inherently does not consider the column rectangularity.

Two attempts are made, in order to incorporate the effect of column rectangularity and the r_{long}/d ratio at once, and the resulting two equations developed within the content of the current investigation are given in Equation 6.19 and Equation 6.20.

$$v_{c2} = 0.18 * \sqrt{\frac{f_c'}{r_{long}/u_{pTS}}} \tag{6.18}$$

$$v_{c3} = 0.18 * \sqrt{\frac{f_c'}{r_{long}/u_{pe}}} \tag{6.20}$$

Since, the punching perimeter calculations inherently contains the slab effective depth, the proposed equations implicitly consider both the concrete strength, column rectangularity and the r_{long}/d ratio of the specimens. The value of experimental shear strength, v_{cts} obtained according to the TS-500 [24] punching perimeter approach; experimental shear strength, v_{ce} obtained according to the new punching perimeter approach outlined in Equation 6.16; the predicted shear strength, v_{TS} according to TS-500 Building Code[24] by Equation 6.5; the predicted shear strength, v_{c1} proposed by Ozden[9]; and the predicted shear strengths, v_{c2} and v_{c3} proposed in the current research are tabulated in Table 6.6 and Table 6.7. For comparison purposes the ratios v_{ce}/v_{TS}, v_{cts}/v_{TS}, v_{cts}/v_{c1}, v_{cts}/v_{c2}, v_{cts}/v_{c3}, v_{ce}/v_{c1}, v_{ce}/v_{c2}, v_{ce}/v_{c3} values are also given in Table 6.7 and plotted in Figure 6.5 to Figure 6.12.

Table 6.5. Specimen properties of the available data

Spc. No.	Ref.	Spcm. Name	D_{sup} (mm)	t (mm)	d (mm)	d' (mm)	r_{long} (mm)	r_{short} (mm)	f_c' (MPa)	f_y (MPa)	D (mm)	s^+ (mm)	s^- (mm)	P_p (kN)
1		OOSW	1720	120	100	20.0	720.0	120.0	24.9	547	10.0	75.0	150.0	359.5
2	[54]	4	1829	152	117		495.0	114.0	31.0	412	15.9	152.4		330.8
3	[54]	8	1829	152	117		495.0	114.0	26.1	414	12.7	133.3		314.8
4		OORC	1480	120	100	20.0	480.0	120.0	24.9	547	10.0	75.0	150.0	327.5
5		OOTE	1464	120	100	20.0	463.0	120.0	24.9	547	10.0	75.0	150.0	347.0
6	[54]	3	1829	152	117		457.0	152.0	32.0	412	15.9	152.4		333.5
7	[54]	5	1829	152	117		457.0	152.0	26.9	412	15.9	65.3		355.3
8	[54]	6	1829	152	117		457.0	152.0	22.7	412	15.9	152.4		336.1
9	[54]	7	1829	152	117		457.0	152.0	25.9	412	15.9	196.9		320.1
10	[12]	R1	1800	152	114		457.2	152.4	27.6	328	15.9	127.0		394.0
11	[54]	9	1829	152	117		305.0	152.0	29.5	414	12.7	139.7		315.6
12	[54]	2	1829	152	117		406.0	203.0	26.4	412	15.9	152.4		351.7
13	[47]	V/Ir/1	850	76.2	55.6	20.6	152.4	76.2	26.7	414	7.9	76.2	76.2	108.7
14	[56]	II/3	1700	100	80		430.0	230.0	17.0	490	8.0	48.0		244.9
15		OOSQ	1300	120	100	20.0	300.0	300.0	24.9	547	10.0	75.0	150.0	353.6
16	[12]	M1A	1800	152	114		304.8	304.8	20.8	481	19.1	165.1		433.2
17	[57]	S-3	597	50.8	38.1		101.6	101.6	26.2	345	6.4	59.0		53.4
18	[54]	1	1829	152	117		305.0	305.0	30.4	412	15.9	152.4		384.2
19	[41]	2S6	864	76.2	63.5		152.4	152.4	19.5	376	6.4	31.8		96.6
20	[41]	3S6	864	76.2	63.5		152.4	152.4	23.0	376	6.4	15.8		150.0
21	[58]	AN-1	1828	146	111		254.0	254.0	18.7	404	15.9	118.6		334.3
22	[47]	V/I/2	850	76.2	55.6	20.6	127.0	127.0	27.6	435	7.9	76.2	76.2	118.0
23	[12]	S1-60	1800	152	114		254.0	254.0	23.3	400	15.9	165.1		389.5
24	[12]	S2-60	1800	152	114		254.0	254.0	22.1	400	15.9	114.3		356.2
25	[12]	S3-60	1800	152	114		254.0	254.0	22.6	400	15.9	76.2		363.9
26	[12]	S4-60	1800	152	114		254.0	254.0	23.8	400	15.9	50.8		333.9
27	[12]	S1-70	1800	152	114		254.0	254.0	24.5	483	15.9	165.1		392.7
28	[12]	S3-70	1800	152	114		254.0	254.0	25.4	483	15.9	76.2		378.4
29	[12]	S4-70	1800	152	114		254.0	254.0	35.2	483	15.9	50.8		374.0
30	[12]	S4A-70	1800	152	114		254.0	254.0	20.5	483	15.9	50.8		311.6
31	[12]	H1	1800	152	114		254.0	254.0	26.1	328	15.9	186.0		371.7
32	[49]	NHZS 1.0	1870	150	119	26.0	250.0	250.0	32.2	400	16.0	170.0	170.0	475.5
33	[49]	NNZS 1.0	1870	150	119	26.0	250.0	250.0	37.2	400	16.0	170.0	170.0	484.8
34	[41]	2S5	864	76.2	63.5		127.0	127.0	23.5	376	6.4	31.8		96.6
35	[9]	NR1E0F0	1200	120	100	20.0	200.0	200.0	21.6	507	10.0	108.0	218.0	187.9
36	[9]	NR2E0F0	1200	120	100	20.0	200.0	200.0	20.0	507	10.0	72.0	145.0	201.6
37	[58]	BN-1	1828	146	111		203.0	203.0	20.2	404	15.9	177.8		265.8
38	[59]	K1	1500	200	180	20.0	300.0	300.0	26.0	568	13.0	80.0	80.0	658.0
39	[41]	2S4	864	76.2	63.5		101.6	101.6	24.6	376	6.4	31.8		85.8
40	[41]	3S4	864	76.2	63.5		101.6	101.6	24.1	376	6.4	15.8		115.2
41	[12]	R2	1800	152	114		152.4	152.4	26.6	328	15.9	127.0		311.6
42	[41]	2S3	864	76.2	63.5		76.2	76.2	26.1	376	6.4	31.8		91.2
43	[41]	2R2	864	76.2	63.5		50.8	50.8	27.6	376	6.4	31.8		81.9
44	[41]	3S2	864	76.2	63.5		50.8	50.8	24.2	376	6.4	15.8		78.5

Table 6.6. Experimental punching shear strengths of available data

Spc. No.	Ref.	Specm.	r_{long}/r_{short} (aspect ratio)	r_{long}/d	a/d	u_{pe} (mm)	a_{1TS} (mm)	u_{pTS} (mm)	v_{ce} (MPa)	v_{cts} (MPa)	v_{TS} (MPa)	v_{c1} (MPa)
1		OOSW	6.00	7.20	5.00	2080.00	240.00	1600.00	1.73	2.25	1.75	1.30
2	[54]	4	4.34	4.22	5.69	1687.20	228.00	1609.20	1.67	1.75	1.95	1.90
3	[54]	8	4.34	4.22	5.69	1687.20	228.00	1609.20	1.59	1.67	1.79	1.74
4		OORC	4.00	4.80	5.00	1600.00	240.00	1600.00	2.05	2.05	1.75	1.59
5		OOTE	3.86	4.63	5.01	1600.00	231.50	1600.00	2.17	2.17	1.75	1.62
6	[54]	3	3.01	3.90	5.85	1687.20	228.50	1687.20	1.68	1.68	1.98	2.01
7	[54]	5	3.01	3.90	5.85	1687.20	228.50	1687.20	1.80	1.80	1.82	1.84
8	[54]	6	3.01	3.90	5.85	1687.20	228.50	1687.20	1.70	1.70	1.67	1.69
9	[54]	7	3.01	3.90	5.85	1687.20	228.50	1687.20	1.62	1.62	1.78	1.80
10	[12]	R1	3.00	4.00	5.87	1676.40	228.60	1676.40	2.06	2.06	1.84	1.84
11	[54]	9	2.01	2.60	6.50	1383.20	152.50	1383.20	1.95	1.95	1.90	2.36
12	[54]	2	2.00	3.46	6.07	1687.20	203.00	1687.20	1.78	1.78	1.80	1.93
13	[47]	V/Ir/1	2.00	2.74	6.27	679.60	76.20	679.60	2.88	2.88	1.81	2.18
14	[56]	II/3	1.87	5.38	7.94	1640.00	215.00	1640.00	1.87	1.87	1.44	1.24
15		OOSQ	1.00	3.00	5.00	1600.00	150.00	1600.00	2.21	2.21	1.75	2.02
16	[12]	M1A	1.00	2.67	6.54	1676.40	152.40	1676.40	2.26	2.26	1.60	1.95
17	[57]	S-3	1.00	2.67	6.50	558.80	50.80	558.80	2.51	2.51	1.79	2.19
18	[54]	1	1.00	2.60	6.50	1689.20	152.50	1689.20	1.94	1.94	1.93	2.39
19	[41]	2S6	1.00	2.40	5.60	863.60	76.20	863.60	1.76	1.76	1.55	2.00
20	[41]	3S6	1.00	2.40	5.60	863.60	76.20	863.60	2.74	2.74	1.68	2.17
21	[58]	AN-1	1.00	2.29	7.09	1460.00	127.00	1460.00	2.06	2.06	1.51	2.00
22	[47]	V/I/2	1.00	2.28	6.50	730.40	63.50	730.40	2.91	2.91	1.84	2.43
23	[12]	S1-60	1.00	2.22	6.76	1473.20	127.00	1473.20	2.31	2.31	1.69	2.27
24	[12]	S2-60	1.00	2.22	6.76	1473.20	127.00	1473.20	2.12	2.12	1.65	2.21
25	[12]	S3-60	1.00	2.22	6.76	1473.20	127.00	1473.20	2.16	2.16	1.66	2.23
26	[12]	S4-60	1.00	2.22	6.76	1473.20	127.00	1473.20	1.98	1.98	1.71	2.29
27	[12]	S1-70	1.00	2.22	6.76	1473.20	127.00	1473.20	2.33	2.33	1.73	2.32
28	[12]	S3-70	1.00	2.22	6.76	1473.20	127.00	1473.20	2.25	2.25	1.76	2.37
29	[12]	S4-70	1.00	2.22	6.76	1473.20	127.00	1473.20	2.22	2.22	2.08	2.79
30	[12]	S4A-70	1.00	2.22	6.76	1473.20	127.00	1473.20	1.85	1.85	1.58	2.13
31	[12]	H1	1.00	2.22	6.76	1473.20	127.00	1473.20	2.21	2.21	1.79	2.40
32	[49]	NHZS 1	1.00	2.10	6.81	1476.00	125.00	1476.00	2.71	2.71	1.99	2.74
33	[49]	NNZS 1	1.00	2.10	6.81	1476.00	125.00	1476.00	2.76	2.76	2.13	2.95
34	[41]	2S5	1.00	2.00	5.80	762.00	63.50	762.00	2.00	2.00	1.70	2.40
35	[9]	NR1E0F0	1.00	2.00	5.00	1200.00	100.00	1200.00	1.57	1.57	1.63	2.30
36	[9]	NR2E0F0	1.00	2.00	5.00	1200.00	100.00	1200.00	1.68	1.68	1.57	2.21
37	[58]	BN-1	1.00	1.83	7.32	1256.00	101.50	1256.00	1.91	1.91	1.57	2.33
38	[59]	K1	1.00	1.67	3.33	1920.00	150.00	1920.00	1.90	1.90	1.78	2.76
39	[41]	2S4	1.00	1.60	6.00	660.40	50.80	660.40	2.05	2.05	1.74	2.74
40	[41]	3S4	1.00	1.60	6.00	660.40	50.80	660.40	2.75	2.75	1.72	2.72
41	[12]	R2	1.00	1.33	7.21	1066.80	76.20	1066.80	2.56	2.56	1.81	3.13
42	[41]	2S3	1.00	1.20	6.20	558.80	38.10	558.80	2.57	2.57	1.79	3.26
43	[41]	2R2	1.00	0.80	6.40	457.20	25.40	457.20	2.82	2.82	1.84	4.11
44	[41]	3S2	1.00	0.80	6.40	457.20	25.40	457.20	2.70	2.70	1.72	3.85

Table 6.7. Calculated punching shear strengths of the available data

Spc. No.	Ref.	Spcm.	v_{c2} (MPa)	v_{c3} (MPa)	v_{ce}/v_{TS}	v_{cts}/v_{TS}	v_{cts}/v_{c1}	v_{cts}/v_{c2}	v_{cts}/v_{c3}	v_{ce}/v_{c1}	v_{ce}/v_{c2}	v_{ce}/v_{c3}	R_i
1		OOSW	1.34	1.53	0.99	1.29	1.73	1.68	1.47	1.33	1.29	1.13	1.15
2	[54]	4	1.81	1.85	0.86	0.90	0.92	0.97	0.95	0.88	0.92	0.90	0.82
3	[54]	8	1.66	1.70	0.89	0.93	0.96	1.01	0.98	0.91	0.96	0.94	0.66
4		OORC	1.64	1.64	1.17	1.17	1.28	1.25	1.25	1.28	1.25	1.25	1.15
5		OOTE	1.67	1.67	1.24	1.24	1.34	1.30	1.30	1.34	1.30	1.30	1.15
6	[54]	3	1.96	1.96	0.85	0.85	0.84	0.86	0.86	0.84	0.86	0.86	0.81
7	[54]	5	1.79	1.79	0.99	0.99	0.98	1.00	1.00	0.98	1.00	1.00	2.05
8	[54]	6	1.65	1.65	1.02	1.02	1.01	1.03	1.03	1.01	1.03	1.03	0.96
9	[54]	7	1.76	1.76	0.91	0.91	0.90	0.92	0.92	0.90	0.92	0.92	0.69
10	[12]	R1	1.81	1.81	1.12	1.12	1.12	1.14	1.14	1.12	1.14	1.14	0.85
11	[54]	9	2.08	2.08	1.02	1.02	0.83	0.93	0.93	0.83	0.93	0.93	0.59
12	[54]	2	1.89	1.89	0.99	0.99	0.92	0.94	0.94	0.92	0.94	0.94	0.89
13	[47]	V/Ir/1	1.96	1.96	1.59	1.59	1.32	1.46	1.46	1.32	1.46	1.46	0.94
14	[56]	II/3	1.45	1.45	1.29	1.29	1.50	1.29	1.29	1.50	1.29	1.29	1.56
15		OOSQ	2.07	2.07	1.27	1.27	1.10	1.07	1.07	1.10	1.07	1.07	1.15
16	[12]	M1A	1.93	1.93	1.42	1.42	1.16	1.17	1.17	1.16	1.17	1.17	1.59
17	[57]	S-3	2.16	2.16	1.40	1.40	1.14	1.16	1.16	1.14	1.16	1.16	0.95
18	[54]	1	2.34	2.34	1.00	1.00	0.81	0.83	0.83	0.81	0.83	0.83	0.83
19	[41]	2S6	1.89	1.89	1.14	1.14	0.88	0.93	0.93	0.88	0.93	0.93	1.34
20	[41]	3S6	2.05	2.05	1.63	1.63	1.26	1.33	1.33	1.26	1.33	1.33	2.47
21	[58]	AN-1	1.87	1.87	1.36	1.36	1.03	1.11	1.11	1.03	1.11	1.11	1.41
22	[47]	V/I/2	2.27	2.27	1.58	1.58	1.19	1.28	1.28	1.19	1.28	1.28	0.97
23	[12]	S1-60	2.09	2.09	1.37	1.37	1.02	1.11	1.11	1.02	1.11	1.11	0.87
24	[12]	S2-60	2.04	2.04	1.29	1.29	0.96	1.04	1.04	0.96	1.04	1.04	1.29
25	[12]	S3-60	2.06	2.06	1.30	1.30	0.97	1.05	1.05	0.97	1.05	1.05	1.91
26	[12]	S4-60	2.11	2.11	1.16	1.16	0.87	0.94	0.94	0.87	0.94	0.94	2.80
27	[12]	S1-70	2.15	2.15	1.35	1.35	1.00	1.09	1.09	1.00	1.09	1.09	1.02
28	[12]	S3-70	2.18	2.18	1.27	1.27	0.95	1.03	1.03	0.95	1.03	1.03	2.18
29	[12]	S4-70	2.57	2.57	1.07	1.07	0.80	0.86	0.86	0.80	0.86	0.86	2.78
30	[12]	S4A-70	1.96	1.96	1.17	1.17	0.87	0.94	0.94	0.87	0.94	0.94	3.64
31	[12]	H1	2.21	2.21	1.23	1.23	0.92	1.00	1.00	0.92	1.00	1.00	0.60
32	[49]	NHZS 1	2.48	2.48	1.36	1.36	0.99	1.09	1.09	0.99	1.09	1.09	0.70
33	[49]	NNZS 1	2.67	2.67	1.29	1.29	0.94	1.03	1.03	0.94	1.03	1.03	0.65
34	[41]	2S5	2.14	2.14	1.18	1.18	0.83	0.93	0.93	0.83	0.93	0.93	1.22
35	[9]	NR1E0F0	2.05	2.05	0.96	0.96	0.68	0.76	0.76	0.68	0.76	0.76	0.79
36	[9]	NR2E0F0	1.97	1.97	1.07	1.07	0.76	0.85	0.85	0.76	0.85	0.85	1.24
37	[58]	BN-1	2.01	2.01	1.21	1.21	0.82	0.95	0.95	0.82	0.95	0.95	0.90
38	[59]	K1	2.32	2.32	1.07	1.07	0.69	0.82	0.82	0.69	0.82	0.82	1.03
39	[41]	2S4	2.28	2.28	1.18	1.18	0.75	0.90	0.90	0.75	0.90	0.90	1.19
40	[41]	3S4	2.25	2.25	1.60	1.60	1.01	1.22	1.22	1.01	1.22	1.22	2.42
41	[12]	R2	2.46	2.46	1.42	1.42	0.82	1.04	1.04	0.82	1.04	1.04	0.87
42	[41]	2S3	2.49	2.49	1.44	1.44	0.79	1.03	1.03	0.79	1.03	1.03	1.15
43	[41]	2R2	2.84	2.84	1.53	1.53	0.69	0.99	0.99	0.69	0.99	0.99	1.12
44	[41]	3S2	2.66	2.66	1.57	1.57	0.70	1.02	1.02	0.70	1.02	1.02	2.41

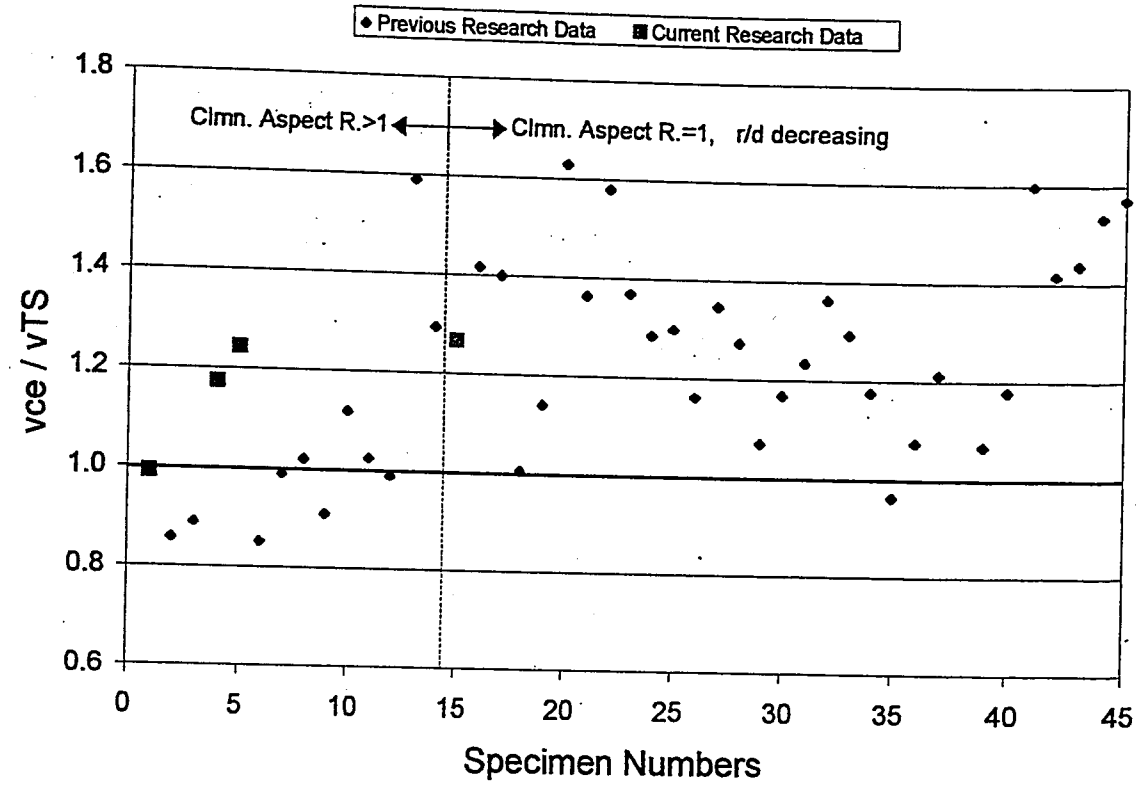

Figure 6.5. Spread of v_{ce}/v_{TS} values for available data

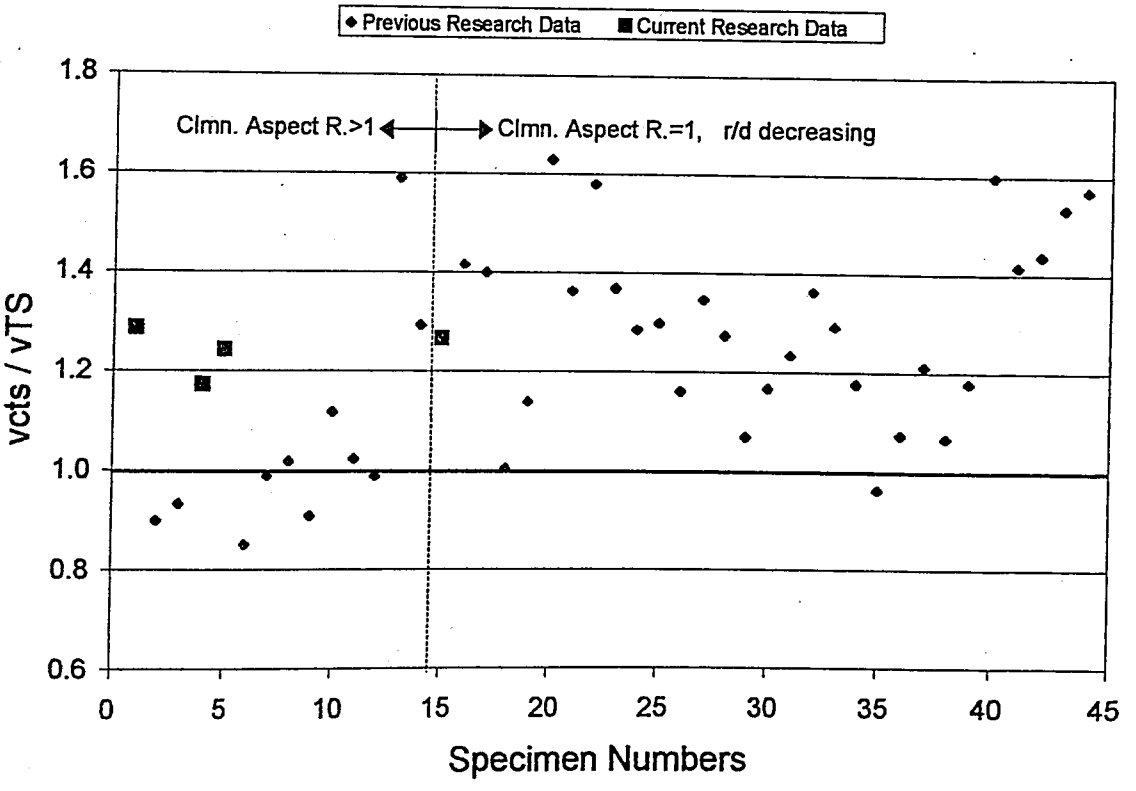

Figure 6.6. Spread of v_{cts}/v_{TS} values for available data

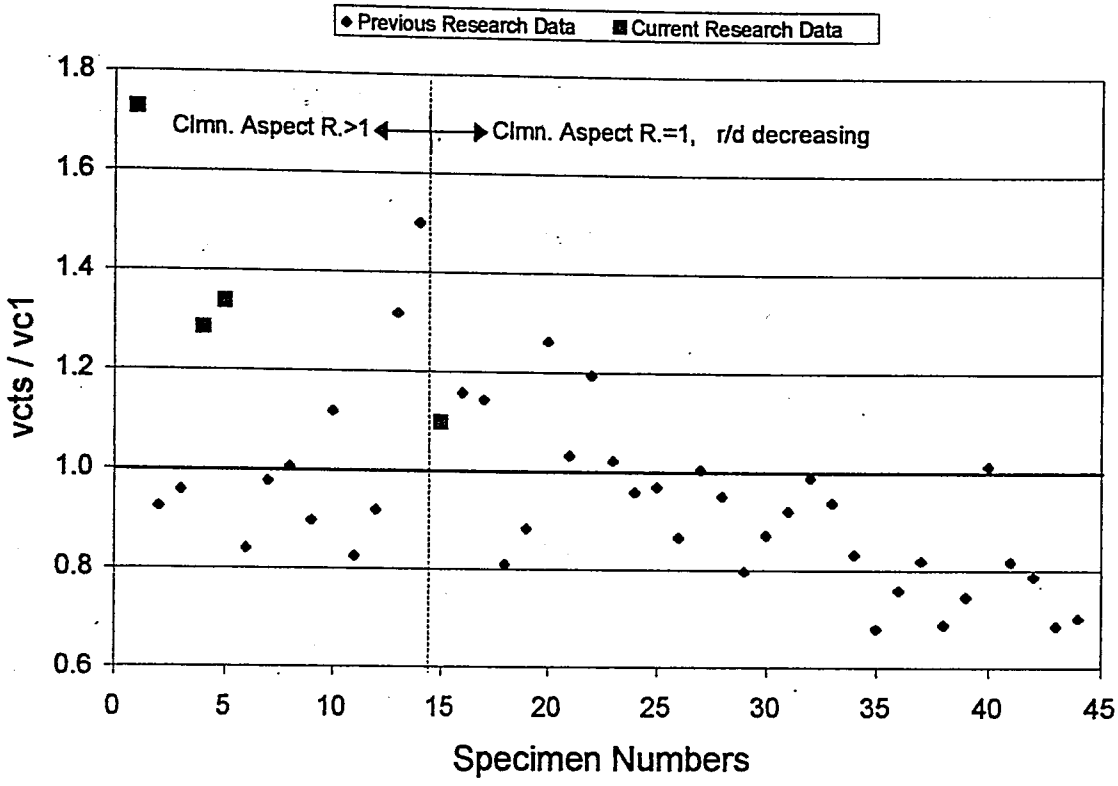

Figure 6.7. Spread of v_{cts}/v_{c1} values for available data

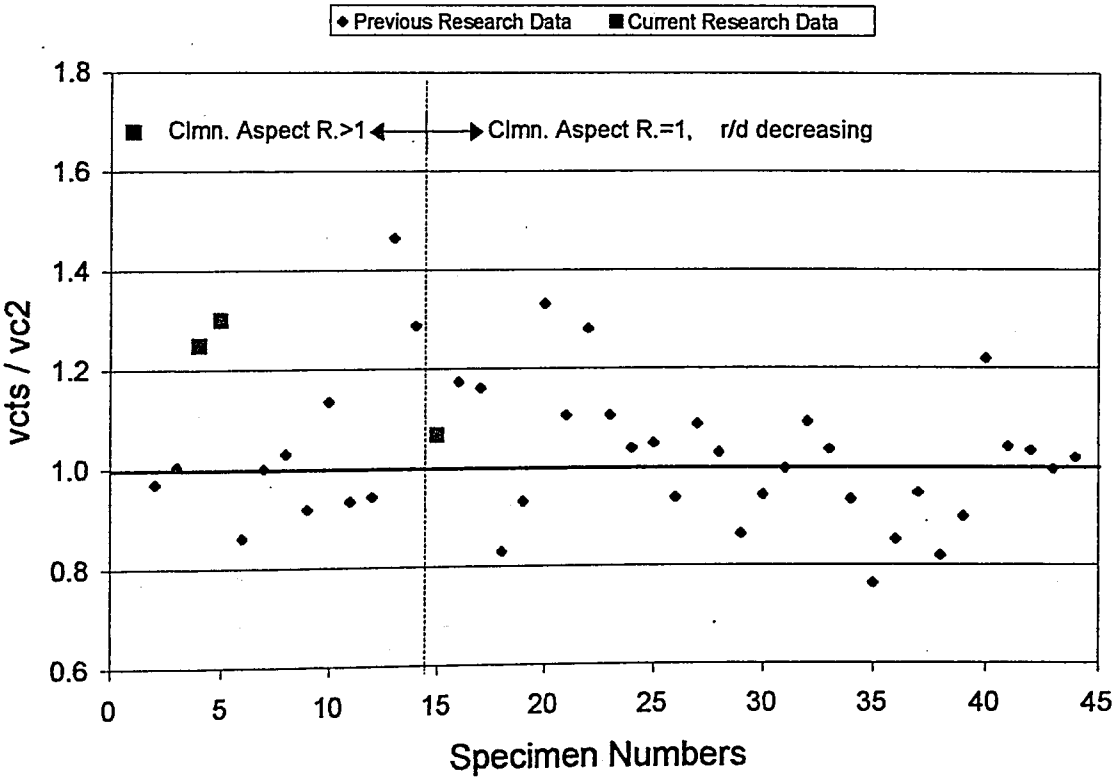

Figure 6.8. Spread of v_{cts}/v_{c2} values for available data

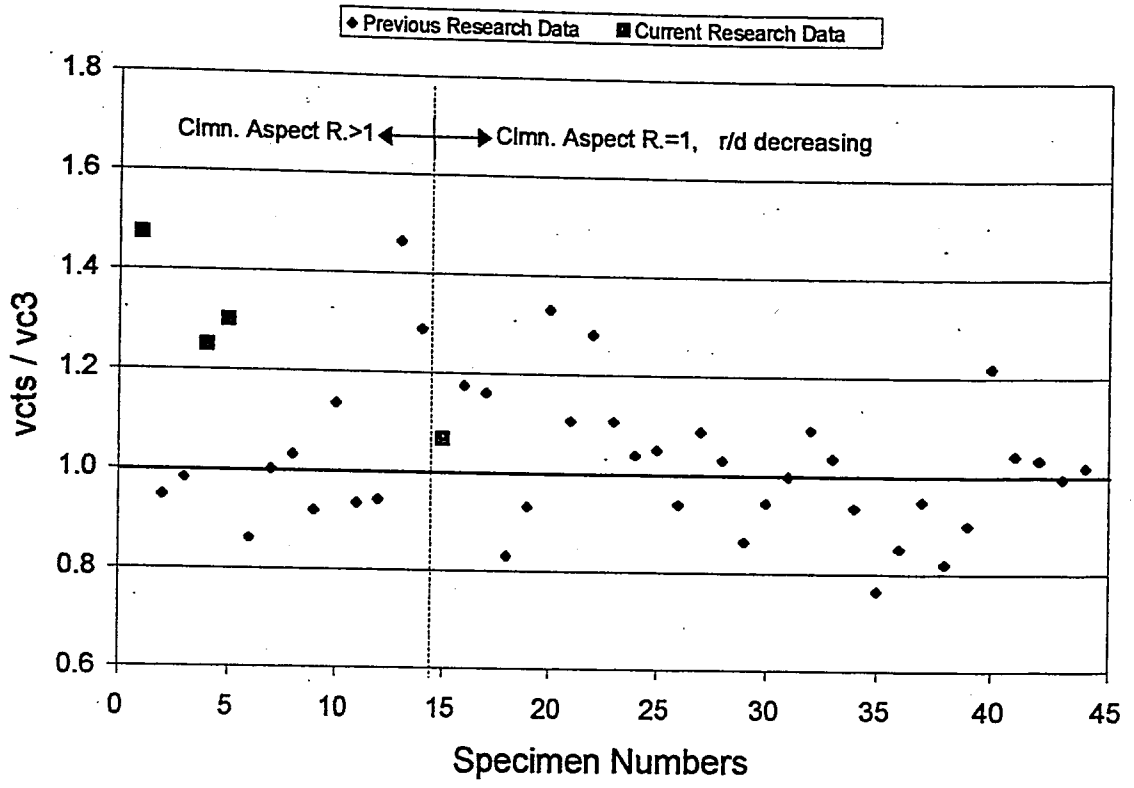

Figure 6.9. Spread of v_{cts}/v_{c3} values for available data

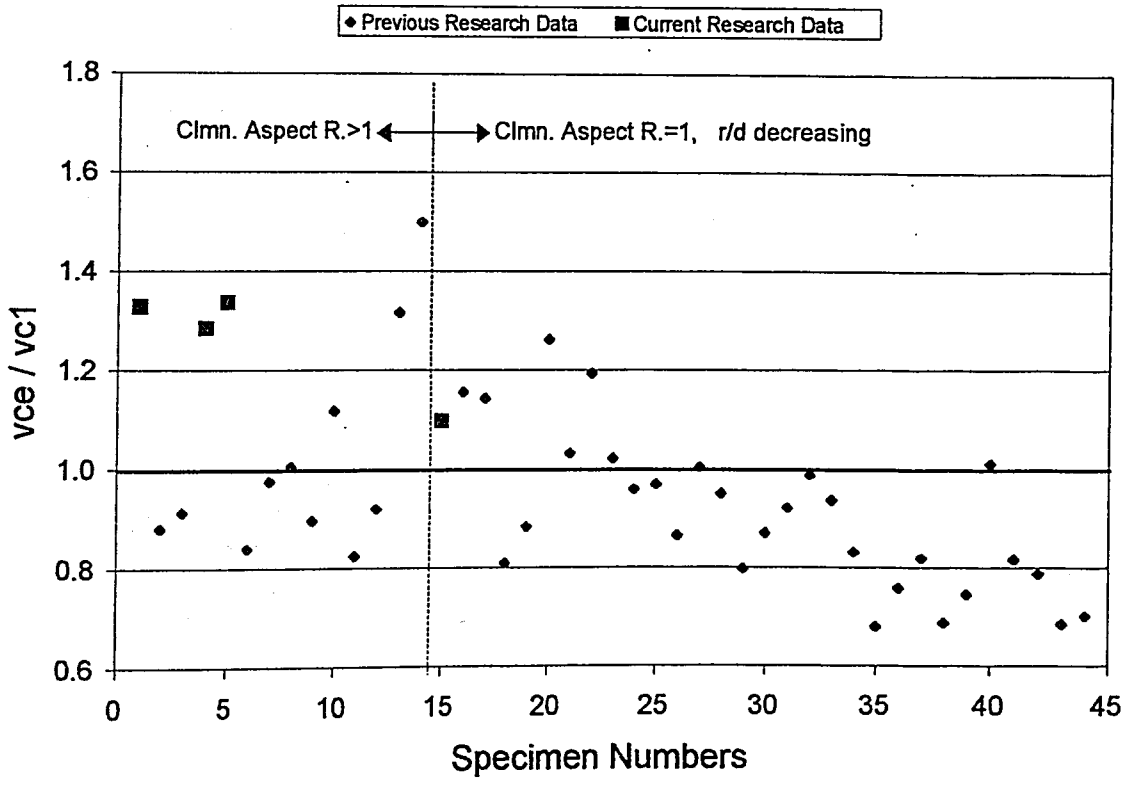

Figure 6.10. Spread of v_{ce}/v_{c1} values for available data

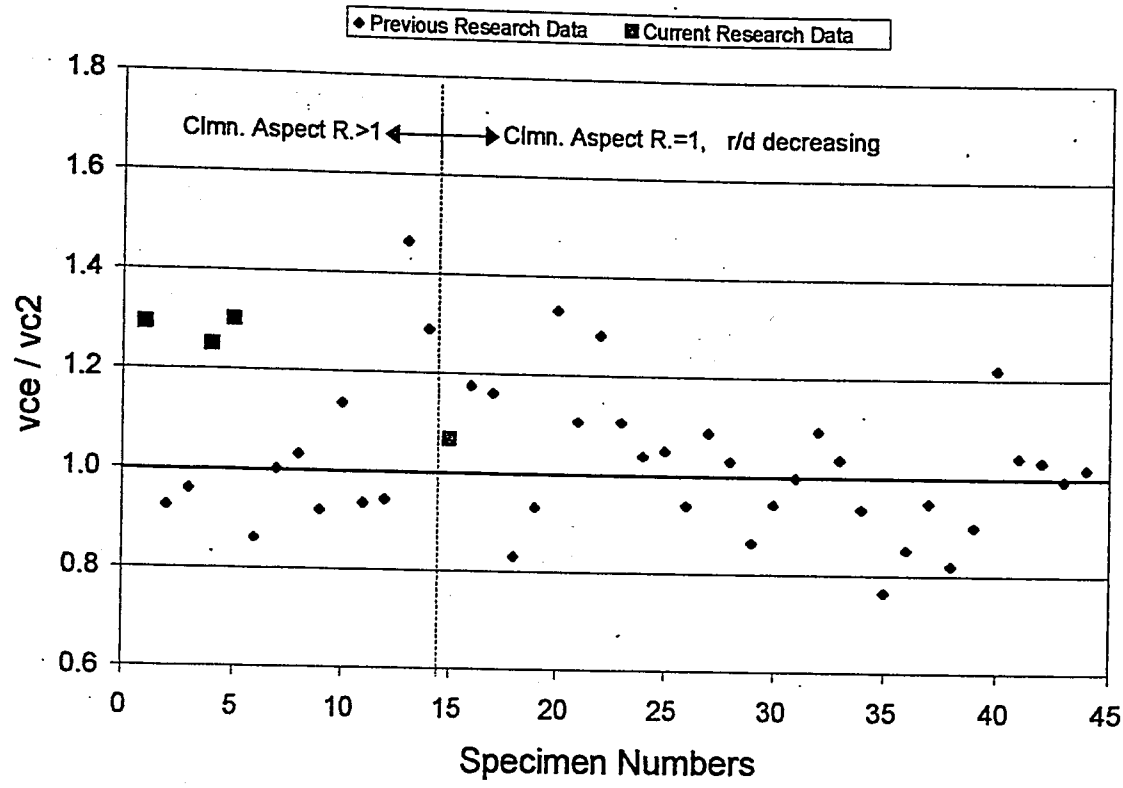

Figure 6.11. Spread of v_{ce}/v_{c2} values for available data

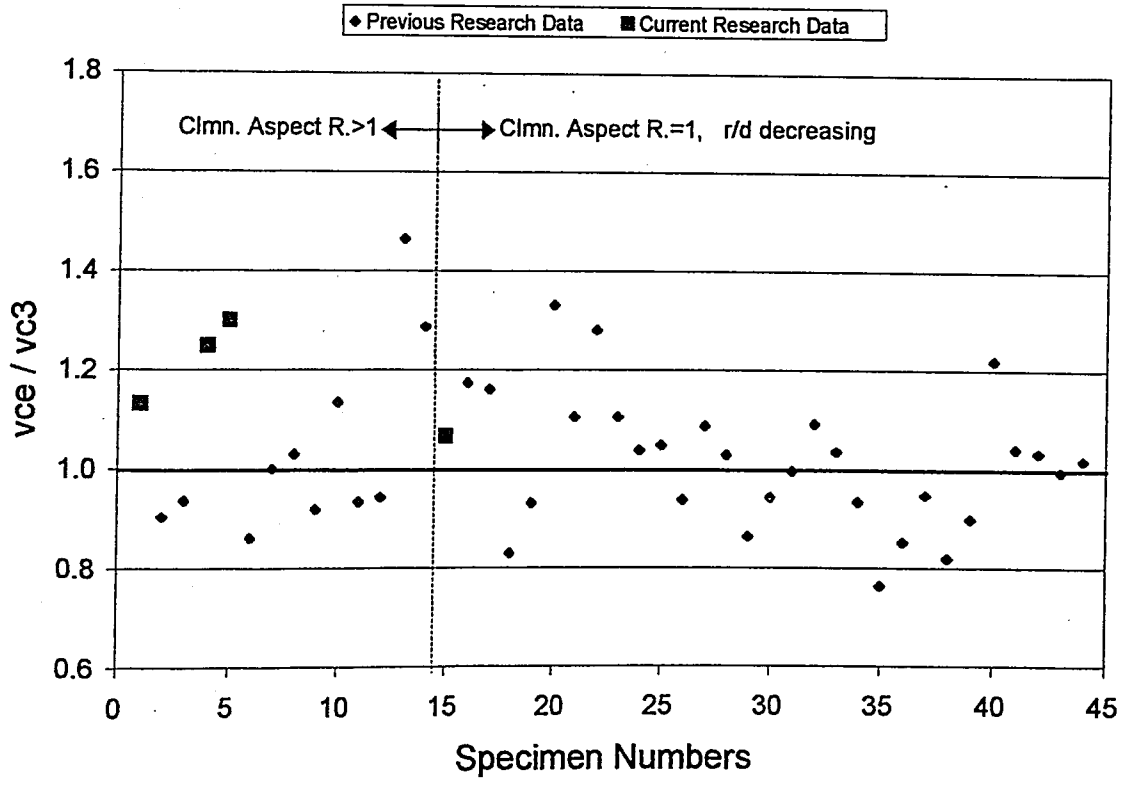

Figure 6.12. Spread of v_{ce}/v_{c3} values for available data

The graphs shown in Figures 6.5 to 6.12 are yielding the ratios of the experimental values to the predicted capacities of the individual specimens. The eight graphs given, need to be statistically evaluated for the best fit in order to choose the most suitable design equation for the punching shear strength calculations.

The data set is divided mainly into two groups; one with column aspect ratio of unity which contains square columns, and the other with column aspect ratio greater than unity which contains the rectangular columns and the shear walls. Mean value, minimum and maximum values, spread of the data points were calculated for these data sets and given in Table 6.8. Beside these statistical values, the sum of absolute value of the errors of each data set with respect to their own mean value was also calculated and listed in the same table.

The TS-500 Building Code [24] approach on punching perimeter determination and shear strength predictions (v_{cts}/v_{TS}) had a spread value of 0.78 and a Σerr of 7.52 for the whole data set. On the other hand, the ratio for the proposed perimeter and strength calculation equations (v_{ce}/v_{c3}) yielded 0.70 and 5.24 for the data spread and Σerr respectively, for the whole data set. As a result, the proposed approach may be considered as more realistic than the available code equations.

When the data set of specimens with square columns only was considered, the code predictions yielded a spread of 0.67 and a Σerr of 4.37, while the proposed approach yielded 0.57 and 3.09, respectively. The same statistical variables were 0.74, 2.23 and 0.60, 2.21 for the code predictions and for the proposed equations, respectively in case of rectangular columns with aspect ratio greater than unity.

Investigation on the predicted and the experimental shear strength of the specimens of the current investigation and of the available test data indicated that, the r_{long}/d and r_{long}/r_{short} ratios had a bearing on the punching strength of the flat plates, and need to be incorporated into the design equations.

Table 6.8. Statistical evaluation of the Figures 6.5 to 6.12

Graph	All Available Data (44 Specimens)					Data with Column Aspect Ratio=1 (30 Specimens)					Data with Column Aspect Ratio>1 (14 Specimens)				
Method	Mean	Min	Max	Spread	Σerr	Mean	Min	Max	Spread	Σerr	Mean	Min	Max	Spread	Σerr
v_{ce}/v_{TS}	1.22	0.85	1.63	0.78	7.78	1.30	0.96	1.63	0.67	4.37	1.07	0.85	1.59	0.74	2.17
v_{cts}/v_{TS}	1.23	0.85	1.63	**0.78**	**7.52**	1.30	0.96	1.63	**0.67**	**4.37**	1.09	0.85	1.59	**0.74**	**2.23**
v_{cts}/v_{c1}	0.98	0.68	1.73	1.05	7.15	0.91	0.68	1.26	0.58	3.88	1.12	0.83	1.73	0.90	3.17
v_{cts}/v_{c2}	1.05	0.76	1.68	0.92	5.75	1.02	0.76	1.33	0.57	3.09	1.13	0.86	1.68	0.82	2.72
v_{cts}/v_{c3}	1.05	0.76	1.47	0.71	5.59	1.02	0.76	1.33	0.57	3.09	1.11	0.86	1.47	0.61	2.52
v_{ce}/v_{c1}	0.97	0.68	1.50	0.82	6.76	0.91	0.68	1.26	0.58	3.88	1.08	0.83	1.50	0.67	2.78
v_{ce}/v_{c2}	1.04	0.76	1.46	0.70	5.36	1.02	0.76	1.33	0.57	3.09	1.09	0.86	1.46	0.60	2.35
v_{ce}/v_{c3}	1.04	0.76	1.46	**0.70**	**5.24**	1.02	0.76	1.33	**0.57**	**3.09**	1.08	0.86	1.46	**0.60**	**2.21**

Σerr = Σ[absolute(Data Point Value – Mean of the Specific Data Set)]

Spread = Max. - Min

7. CONCLUSIONS

The following conclusions may be drawn as a result of the research outlined above:

- In all of the four specimens, regardless of the column x-sectional aspect ratio, the punching failure occurred suddenly. The failure was abrupt and brittle. After the punching failure, the concentric load capacity of the plate-to-column connection dropped suddenly.

- Beyond the failure load, another force equilibrium point was reached. This level of capacity, at which the plate could carry the load under increasing center deflections, may be called residual load level.

- The shear stress over a punching perimeter at the time of failure is comparable in all of the specimens, the rectangular plate-to-column connection yielding the lowest value. The experimentally obtained shear strength level degrades from the case of square column to the case of rectangular column, and raise up to the level of square column again in the case of shear wall specimen.

- The punching load capacity predictions, via TS-500 Building Design Code equations yielded safe results, the safety margin being around 25 percent.

- Stiffness degradation of the plate-to-column connection was studied by comparing the tangent and secant stiffness values with the initial stiffness value. It was observed that, the tangent and the secant stiffnesses were approximately 25 and 35 percent of the initial stiffness, respectively.

- The investigation on the energy absorption at successive 20 percent load increments that of the punching capacity indicates that, highest energy was absorbed between 40 to 60 percent load level. This may indicate that, the largest plastic deformation at the plate-to-column connection occurs at this load level.

- The residual load levels of the plate-to-column connections with higher column rectangularity may well be predicted by the equations proposed in the previous Boğaziçi research.

- The punching capacity calculation of the connection may be refined by using the column rectangularity in the theoretical shear strength predictions as given in Equation 6.17 and Equation 6.20 of the current investigation.

- The compression side of the flat plates remained uncracked and uncrushed until the punching failure took place.

- The crack patterns on the tension side of the specimens resemble the shape of the column stub. The cracks are intensified around the column shorter sides.

- The flexural crack, which became the punching crack when the punching load was reached, was located at a distance of "d" from the column stub.

REFERENCES

1. Ersoy, U., T. Erdogan and T. Tankut, *Investigation Report on the Failure of ASELSAN Building Submitted to Court, File N. Hz.981-5531*, 17 pp., November 1981 (in Turkish).

2. Ersoy, U., *Report on Bayrampasa Wholesale Food Market Building* January 14, 1986 (in Turkish).

3. "Building Collapse Blamed on Design, Construction," *Engineering News Record*, p.19, July 15, 1971.

4. Pan, A.P. and J.P. Moehle, *Reinforced Concrete Flat Plates under Lateral Loading: An Experimental Study Including Biaxial Effects* Report No UCB/EERC-88/16, Eartquake Engineering Research Center, University of California at Berkeley, 262 pp., October 1988.

5. Sozen, M.A. *Selection of Flexural Reinforcement in Reinforced Concrete Flat Slabs/Plates* University of Illinois, Urbana, Illinois, March 1992.

6. Peabody, D. *The Design of Reinforced Concrete Structures* John Wiley & Sons, 532.p., Second Edition, 1946.

7. ERSOY, U. *Reinforced Concrete 2: Slabs & Footings* Evrim Yayinevi, Istanbul Turkey, 245p., First Edition, 1995 (in Turkish).

8. Sozen, M.A. and C.P. Siess, "Investigation of Multi-Panel R/C Floor Slabs: Design Methods, Their Evaluation and Comparison," *ACI Journal*, V.60, N.8, August 1963.

9. Ozden, S. *Punching Shear Behavior of Normal and High-Strength Concrete Flat-Plates* Ph.D. Thesis, Department of Civil Engineering, Bogaziçi University, Istanbul, Turkiye, 1998.

10. Westergaard, H.M. and W.A. Slater, "Moments and Stresses in Slabs," *ACI Journal, Proceedings*, V.17, pp.415-538, 1921.

11. Hatcher, D.S., M.A. Sozen and C.P. Siess, *A Study of Tests on Flat Plate and a Flat Slab*, Research Report, Civil Engineering Department, University of Illinois, Urbana, Illinois, 143 pp., July 1961.

12. Moe, J. *Shearing Strength of Reinforced Concrete Slabs and Footings Under Concentrated Loads* Development Department Bulletin, N.47, Portland Cement Association, Skokie, 130 pp., April 1961.

13. Hanson, N.W. and J.M. Hanson, "Shear and Moment Transfer Between Concrete Slabs and Columns," *Journal, Portland Cement Association, Research and Development Laboratories*, V.10, N.1, pp.2-16, January 1968.

14. Ozselcuk, A. *Contribution of Flexural Steel to Punching Strength* M.S. Thesis, Department of Civil Engineering, Middle East Technical University, Turkey, 55 pp , 1980.

15. Halgren, M. and S. Kinnunen, "Punching Shear Tests on Circular High Strength Concrete Slabs," *Utilization of High Strength Concrete, Proceedings, Symposium*, Norway, pp.192-199, June 20-23, 1993.

16. Tankut, T. and C.W. Yu, *An Investigation into the Behaviour of Flat Plate Structures* Research Report, Imperial College, London, January, 40 pp., 1969.

17. Pecknold, D.A. "Slab Effective Width for Equivalent Frame Analysis," *ACI Journal, Proceedings*, V.72, N.4, pp.135-137, April 1975.

18. Ertaş, O. *Punching Shear Behavior of Normal Strength Concrete Flat-Plates under Reversed Cyclic Loading* MS. Thesis, Department of Civil Engineering, Bogaziçi University, Istanbul, Turkiye, 2000.

19. Simeonov, B. and E. Gorgievska, "Experimental Investigation of Flat-Plate Models Under Cyclic Loading," *Proceedings of the 8th European Conference on Earthquake Engineering*, V.4, Lisbon, 1986, pp.7.3/9-7.3/16.

20. Morrison, D., I. Hirasawa and F. Allen "The Response of Reinforced Concrete Plate-Column Assemblies Subjected to Horizontal Loading," *Proceedings of the 7th World Conference on Earthquake Engineering*, V.6, Istanbul, Turkey, pp.427-430, September 1980.

21. ACI-ASCE Committe 352 "Recommendations for Design of Slab-Column Connections in Monolithic Reinforced Concrete Structures," (ACI 352.1R-88) *ACI Structural Journal*, V.84, N.6, pp.675-696, November-December 1988.

22. Marzouk, H. and A. Hussein, "Experimental Investigation on the Behavior of High-Strength Concrete Slabs," *ACI Structural Journal*, V.88, N.6, pp.701-713, November-December 1991.

23. ACI-318-95, Building Code Requirements for Reinforced Concrete, American Concrete Institute, Detroit, Michigan.

24. TS-500, Building Code Requirements for Reinforced Concrete, Turkish Standards, April 1984 (in Turkish).

25. Gardner, N.J. "Relationship of the Punching Shear Capacity of Reinforced Concrete Slabs with Concrete Strength," *ACI Structural Journal*, V.87, N.1, pp.66-71, January-February 1990.

26. ASCE-ACI Task Committee 426 "The Shear Strength of Reinforced Concrete Members - Slabs," *Proceedings, ASCE*, V.100, ST8, pp.1543-1951, August 1974.

27. Ramdane, K.E. "Punching Shear of High Performance Slabs," *Fourth International Symposium on the Utilization of High Strength / High Performance Concrete*, Paris, France, pp.1015-1026, V.3, 29-31 May 1996.

28. Gomes, R.B. and M.A.S. Andrade, "The Use of High Performance Concrete in Punching Failure of Reinforced Concrete Flat Slabs," *Fourth International Symposium on the Utilization of High Strength / High Performance Concrete*, Paris, France, pp.1027-1035, V.3, 29-31 May 1996.

29. Park, R. and S. Islam, "Strength of Slab-Column Connections with Shear and Unbalanced Flexure," *Proceedings, ASCE*, V.102, ST9, pp.1879-1901, September 1976.

30. Aoki, Y. and H. Seki, "Shearing Strength and Cracking in Two-Way Slabs Subjected to Concentrated Loads," *Cracking, Deflection, and Ultimate Load of Concrete Slab Systems*, ACI Publication, SP-30, pp.103-127, Detroit, Michigan, 1971.

31. Whitney, C.S. "Ultimate Shear Strength of Reinforced Concrete Flat Slabs, Footings, Beams, and Frame Members without Shear Reinforcement," *ACI Journal, Proceedings*, V.54, N.4, pp.265-298, October 1957.

32. Yitzhaki, D. "Punching Strength of Reinforced Concrete Slabs," *ACI Journal, Proceedings*, V.63, N.5, pp.527-542, May 1966.

33. Zaghlool, E.R.F. and H.A.R. Paiva, "Test of Flat Plate Corner Column-Slab Connections," *Proceedings, ASCE*, V.99, ST3, pp.551-572, March 1973.

34. Neth, V.W., H.A.R. De Paiva and A.E. Long, A.E. "Behavior of Models of Reinforced Concrete Flat Plate Edge-Column Connections," *ACI Journal*, V.78, N.4, pp.269-275, July-August 1981.

35. Shehata, I.A.E.M. and P.E. Regan, "Punching in R.C. Slabs," *Journal, Engineering Structures Division, ASCE*, V.115, N.7, pp.1726-1740, July 1989.

36. Alexander, Scott D.B. and Sidney H. Simmonds, "Tests of Column-Flat Plate Connections," *ACI Structural Journal*, V.89, N.5, pp.495-502, September-October 1992.

37. Paramasivam, P. and K.H. Tan, "Punching Shear Strength of Ferrocement Slabs," *ACI Structural Journal*, V.90, N.3, pp.294-301, May-June 1993.

38. Vanderbilt, M.D. "Shear Strength of Continuos Plates," *Journal of the Structural Division, ASCE*, V.89, N.5, pp.961-973, May 1972.

39. Rankine, G.I.B. and A.E. Long "Predicting the Punching Strength of Conventional Slab-Column Specimens," *Proceedings, Institution of Civil Engineers, Part 1*, 82, pp.327-346, 1987.

40. Fang, I-K., J.H. Lee and C.R. Chen, "Behaviour of Partially Restrained Slabs Under Concentrated Load," *ACI Structural Journal*, V.91, N.2, pp.133-139, March-April 1994.

41. Taylor, R. and B. Hayes, "Some Tests on the Effect of Edge Restraint on Punching Shear in Reinforced Concrete Slabs," *Magazine of Concrete Research*, V.17, N.50, pp.39-44, March 1965.

42. Hawkins, N.M. "Seismic Response of Reinforced Concrete Flat Plate Structures," *Proceedings of the 7th Worl Conference on Earthquake Engineering*, V.4, pp.33-40, Turkey, September 1980.

43. Moehle, J.P., M.E. Kreger and R. Leon, "Background to Recommendations for Design of Reinforced Concrete Slab-Column Connections," *ACI Structural Journal*, V.85, N.6, pp.636-644, November-December 1988.

44. Hawkins, N.M. and W.G. Corley, "Transfer of Unbalanced Moment and Shear from Flat Plates," *Cracking, Deflection, and Ultimate Load of Concrete Slab Systems*, ACI Publication, SP-30, pp.147-176, Detroit, Michigan, 1971.

45. Mitchell, D. and W.D. Cook,. "Preventing Progressive Collapse of Slab Structures," *Journal of Structural Engineering, ASCE*, V.110, N.7, pp.1513-1532, July 1984.

46. Pillai, U. S., W. Kirk and L. Scavuzzo,. "Shear Reinforcement at Slab Column Connections in a Reinforced Concrete Flat Plate Structure," *ACI Journal*, V.79, N.1, pp.36-42, January-February 1982.

47. Stamenkovic, A. and J.C. Chapman, "Local Strength at Column Heads in Flat Slabs Subjected to Combined Vertical and Horizontal Loading," *Proceedings, Institution of Civil Engineers (London)*, Part 2, V.57, pp.205-232, June 1974.

48. Rangan, V.B. "Tests on Slabs in the Vicinity of Edge Columns," *ACI Structural Journal*, V.87, N.6, pp.623-629, November-December 1990.

49. Marzouk, H., M. Emam and M.S. Hilal, "Effect of High-Strength Concrete Columns on the Behaviour of Slab-Column Connections," *ACI Structural Journal*, V.93, N.5, pp.545-554, September-October 1966.

50. Moehle, J.P. and J.W. Diebold, *Experimental Study of the Seismic Response of a Two-Story Flat Plate Structure* UCB/EERC Report No 84/8, University of California - Berkeley, 244 pp., August 1984.

51. Rao, G.R. and H.B. Goli, "Yield Line Analysis of Single Panel Flat Slab," *International Journal of Structures*, V.5, N.1, pp.23-44, January-March 1985.

52. ACI Committee 363 "State-of-the-Art Report on High-Strength Concrete," *Journal of the ACI, Proceedings*, V.81, N.4, pp.364-411, July-August 1984.

53. Kuang, J.S. and C.T. Morley, "Punching Shear Behaviour of Restrained Reinforced Concrete Slabs," *ACI Structural Journal*, V.89, N.1, pp.13-19, January-February 1992.

54. Hawkins, N.M. and D. Mitchell, "Progressive Collapse of Flat Plate Structures," *ACI Journal, Proceedings*, V.76, N.7, pp.775-808, July 1979.

55. Simmonds, S.H. "Slabs Supported on Columns Elongated in Plan" *ACI Journal*, December 1970, pp.967,975.

56. Rosenthal, I. "Experimental Investigation of Flat Plate Floors," *ACI Journal, Proceedings*, 1959-1960, V.56, pp.153-166, August 1959.

57. Ersoy, U. *Ultimate Shearing Strength of Reinforced Concrete Slabs and Footings* R.C. Reese & Associates, Study Proceeding the Report Submitted to Michigan Court, 50 pp. August 10, 1962.

58. Corley, W.G. and N.M. Hawkins, "Shearhead Reinforcement for Slabs," *ACI Journal, Proceedings*, V.65, N.10, pp.811-824, October 1968.

59. Yamada, T., A. Nanni, and K. Endo, "Punching Shear Resistence of Flat Slabs: Influence of Reinforcement Type and Ratio," *ACI Structural Journal*, V.89. N.5, pp.555-563, September-October 1992.